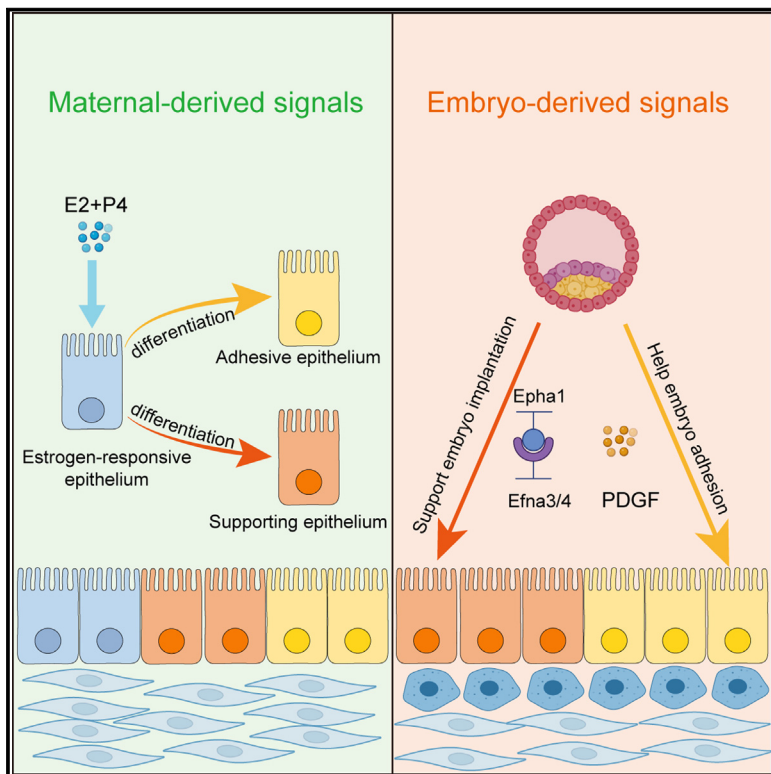


Developmental Cell

Maternal and embryonic signals cause functional differentiation of luminal epithelial cells and receptivity establishment

Graphical abstract



Authors

Hai-Quan Wang, Yang Liu, Dong Li, ..., Chao-Jun Li, Gui-Jun Yan, Hai-Xiang Sun

Correspondence

zhibin_hu@njmu.edu.cn (Z.-B.H.), lichaojun@njmu.edu.cn (C.-J.L.), yanguijun@nju.edu.cn (G.-J.Y.), stevensunz@163.com (H.-X.S.)

In brief

Wang et al. identify maternal and embryonic signals regulating endometrial epithelial cell differentiation and activity during peri-implantation period. They showed that this process is conserved in humans and mice, and defects in endometrial epithelial cells are associated with thin endometrium and recurrent implantation failure.

Highlights

- A transcriptional single-cell census during peri-implantation period in mice
- Maternal signals control endometrial epithelial cell differentiation
- Embryonic signals activate adhesive and supporting epithelial cells
- Epithelial cell defects contribute to thin endometrium and RIF

Resource

Maternal and embryonic signals cause functional differentiation of luminal epithelial cells and receptivity establishment

Hai-Quan Wang,^{1,5} Yang Liu,^{1,3,5} Dong Li,^{1,4,5} Jing-Yu Liu,^{2,4,5} Yue Jiang,^{1,4,5} Yuanlin He,² Ji-Dong Zhou,^{1,4} Zhi-Long Wang,^{1,4} Xin-Yi Tang,^{1,4} Yang Zhang,^{1,4} Xin Zhen,^{1,4} Zhi-Wen Cao,^{1,4} Xiao-Qiang Sheng,^{1,4} Chao-Fan Yang,¹ Qiu-Ling Yue,^{1,4} Li-Jun Ding,^{1,4} Ya-Li Hu,^{1,4} Zhi-Bin Hu,^{2,*} Chao-Jun Li,^{1,2,*} Gui-Jun Yan,^{1,3,4,*} and Hai-Xiang Sun^{1,2,4,6,*}

¹Center for Reproductive Medicine and Obstetrics & Gynecology, Nanjing Drum Tower Hospital, Affiliated Hospital of Medical School, Nanjing University, Nanjing 210008, China

²State Key Laboratory of Reproductive Medicine and Offspring Health Center for Global Health, School of Public Health, Nanjing Medical University, Nanjing 211166, China

³Department of Reproductive Medicine Center, Nanjing Drum Tower Hospital, State Key Laboratory of Pharmaceutical Biotechnology, Nanjing University, Nanjing 210023, China

⁴Center for Molecular Reproductive Medicine, Nanjing University, Nanjing 210008, China

⁵These authors contributed equally

⁶Lead contact

*Correspondence: zhibin_hu@njmu.edu.cn (Z.-B.H.), lichaojun@njmu.edu.cn (C.-J.L.), yanguijun@nju.edu.cn (G.-J.Y.), stevensunz@163.com (H.-X.S.)

<https://doi.org/10.1016/j.devcel.2023.08.004>

SUMMARY

Embryo implantation requires temporospatial maternal-embryonic dialog. Using single-cell RNA sequencing for the uterus from 2.5 to 4.5 days post-coitum (DPC) and bulk sequencing for the corresponding embryos of 3.5 and 4.0 DPC pregnant mice, we found that estrogen-responsive luminal epithelial cells (EECs) functionally differentiated into adhesive epithelial cells (AECs) and supporting epithelial cells (SECs), promoted by progesterone. Along with maternal signals, embryonic *Pdgfa* and *Efna3/4* signaling activated AECs and SECs, respectively, enhancing the attachment of embryos to the endometrium and furthering embryo development. This differentiation process was largely conserved between humans and mice. Notably, the developmental defects of SOX9-positive human endometrial epithelial cells (similar to mouse EEC) were related to thin endometrium, whereas functional defects of SEC-similar unciliated epithelial cells were related to recurrent implantation failure (RIF). Our findings provide insights into endometrial luminal epithelial cell development directed by maternal and embryonic signaling, which is crucial for endometrial receptivity.

INTRODUCTION

Successful embryo implantation requires precise interactions between a receptive endometrium and an activated blastocyst in mammals. Although the details of implantation-related events vary between species, the central roles played by estrogen and progesterone in controlling early pregnancy are common to many mammals.¹ Under the sequential guidance of ovarian estrogen and progesterone, the endometrium becomes conducive to accept a blastocyst for implantation, which is called “receptivity.” In humans, the receptive state spans 7–10 days after the ovulation luteinizing hormone surge, and spontaneous stromal cell decidualization is an indispensable step for receptivity establishment, whereas in mice, it lasts less than 24 h starting 3.5 days post-coitum (DPC, 0.5 DPC = vaginal plug), and decidualization is induced by implantation.^{2,3}

During the process of embryo implantation, the endometrial luminal epithelium is the first maternal tissue that builds phys-

ical interactions with the blastocyst, and orchestrated regulation of the luminal epithelium is critical for the establishment of successful pregnancy. Estrogen induces the proliferation of the epithelium, whereas later progesterone counteracts the estrogen-induced effects.⁴ Under the circumstances of progesterone, some adhesion molecules, such as selectin oligosaccharide-based ligands and integrin $\alpha_v\beta_3$, are upregulated in the epithelium during receptivity to act as modulators of the endometrium-blastocyst interaction,^{5,6} and blockade of integrin $\alpha_v\beta_3$ prevents implantation in mice.⁷ Embryo-derived signals also affect epithelial functions and facilitate embryo implantation. After entering the uterine cavity, the embryo secretes various signaling molecules, including growth factors (such as platelet-derived growth factor [PDGF]), hormones (such as chorionic gonadotropin), and cytokines (such as tumor necrosis factor alpha [TNF- α]), which cause dramatic changes at the molecular and cellular levels.^{8–11} Another fact that should be kept in mind is that epithelial heterogeneity exists, such as

that it can be divided into ciliated epithelium and unciliated epithelium in humans,¹² and another study found that the ciliated epithelial cells could bind with embryos by galectin-glycan, which may mean other potential epithelial-embryo crosstalk,¹³ whereas no such epithelial cells have been found in mice, but the function and regulatory mechanism of epithelial subclusters and the effects of embryo-derived signals on them are far from being understood.

Although some of the changes in endometrial cell activities during peri-implantation mentioned above have been identified, how temporal and cell-specific dynamic alterations are sequentially regulated by maternal and embryogenic signaling is largely unknown because of the cellular complexity and dynamic changes in both the embryo and endometrium. To explore the coordinated regulation of maternal and embryogenic signaling and their effects on the dynamic changes in endometrial cells during peri-implantation, we collected mouse uteri at 2.5, 3.5, 4.0, and 4.5 DPC and the same number of days of pseudopregnant (DPP) for use in single-cell RNA sequencing (scRNA-seq) and embryos from the mouse uterus at 3.5 and 4.0 DPC for use in bulk RNA-seq. These samples were harvested from the time of endometrium preparation to embryo implantation. Mouse embryos are still in the oviduct at 2.5 DPC, when the endometrium is under the sole effect of maternal signaling. Thus, after embryos enter the uterus at 3.5 DPC or later, the endometrium receives signals from both the mother and embryo, which can be distinguished by comparing the pregnant mouse uterine data with the pseudopregnant uterine data.

Because of advances in scRNA-seq technology,¹⁴ we identified the sequential differentiation of endometrial luminal epithelial cells associated with embryo implantation, which was controlled by maternal steroid hormones at 2.5 DPC. Through bioinformatics analyses, we identified cell communication between embryos and luminal epithelial cells from 3.5 to 4.5 DPC and identified embryo-derived peptide signaling that regulated blastocyst adhesion to luminal epithelial cells and embryo implantation. Furthermore, based on these findings in mice, we summarize the characteristics of the luminal epithelium in the endometrium from patients with thin endometrium and recurrent implantation failure (RIF), which may offer new insights into the treatment of these diseases.

RESULTS

Endometrial luminal epithelial cells show dramatic transcriptomic changes during embryo implantation

To investigate the dynamic changes in all uterine cell types during embryo implantation, we compared the single-cell transcriptome profiles of mouse uteri at 4.0 DPC (when embryos were undergoing implantation) and 4.0 DPP (without embryo stimulation) (Figure 1A). We identified 13 clusters in the uteri at 4.0 DPC based on known markers (Figures 1B and 1C). These clusters were grouped into six main cellular categories: (1) epithelial cells, (2) stromal cells, (3) smooth muscle cells, (4) endothelial cells, (5) mesothelial cells, and (6) immune cells (*Ctss*+ monocytes and neutrophils were captured so insufficiently and were excluded from our further analysis). Furthermore, we observed more proliferative stromal cells and fewer

B cells in pregnant uteri than pseudopregnant uteri (Figure 1D). Additionally, cell activity comparison through transcriptomes indicated that epithelial cells, including luminal and glandular epithelial cells, exhibited the most significant alterations in differentially expressed genes (DEGs) (Figure 1E). Gene ontology (GO) analysis showed that compared with 4.0 DPP, there were dynamic changes in protein translation and processing at 4.0 DPC in glandular and luminal epithelial cells, endothelial cells, smooth muscle cells, and some immune cells, which may be associated with the impact of embryo implantation (Figure 1F). Notably, the luminal epithelium physically contacts the embryo in the uterus first; hence, we focused on the difference in the luminal epithelium transcriptome between the pregnant and pseudopregnant groups. Our results showed that some processes related to embryo adhesion were upregulated in the luminal epithelium of the pregnancy groups (Figure 1F). These findings suggest that the endometrial epithelium, especially the luminal epithelium, undergoes dynamic transcriptomic changes in the presence of embryos, although there is no significant change in the size of the population of epithelial cells (Figure 1D).

A single-cell census of the whole mouse uterus during the peri-implantation period

To investigate the signals from both the mother and the fetus acting on the uterus, we prepared two female mice for each designated time stage (2.5, 3.5, 4.0, and 4.5 DPC) as pregnancy groups. We collected one-half of the bicornuate uterus from each pregnant mouse, pooled them, and performed scRNA-seq. To distinguish the effects of maternal and embryonic signaling, we also collected the uteri of pseudopregnant mice at corresponding time points (2.5, 3.5, 4.0, and 4.5 DPP) for scRNA-seq (Figure 2A).

After quality control (QC) filtering, we obtained 71,682 cells for downstream analysis. We grouped the cells into 11 clusters based on the expression of known markers of different cell types (Figures 2B and 2C). Batch effects were generally eliminated, as shown in Figure 2D. We compared the cell ratio of different clusters in the pregnant and pseudopregnant mice at different time points and found significant differences in the cell ratio of multiple cell types (Figure 2E). For example, there was a dramatic decrease in B cells in pregnant uteri from 2.5 to 4.5 DPC, consistent with the establishment of immune tolerance as the pregnancy progressed, whereas the ratio of B cells increased in the pseudopregnant uteri. Interestingly, the ratio of proliferating stromal cells progressively increased in the uteri of pregnant mice but decreased in the uteri of pseudopregnant mice, which suggested that these cells may be related to decidualization. Moreover, the DEG counts of all dominant cell types in the uterus (luminal epithelial cells, *Mki67*(-) stromal cells, *Mki67*(+) stromal cells, and glandular epithelial cells) were calculated between pregnancy and pseudopregnancy groups at each time point, and the luminal epithelium and glandular epithelium exhibited the most significant changes (Figure 2F). To distinguish luminal and glandular epithelial cells, we identified *Tacstd2* as a specific marker for luminal epithelial cells and *Prss29* as a specific marker for glandular epithelial cells and verified their specificity through immunohistochemistry and *in situ* hybridization (ISH), respectively (Figure 2G).

Developmental Cell Resource

CellPress

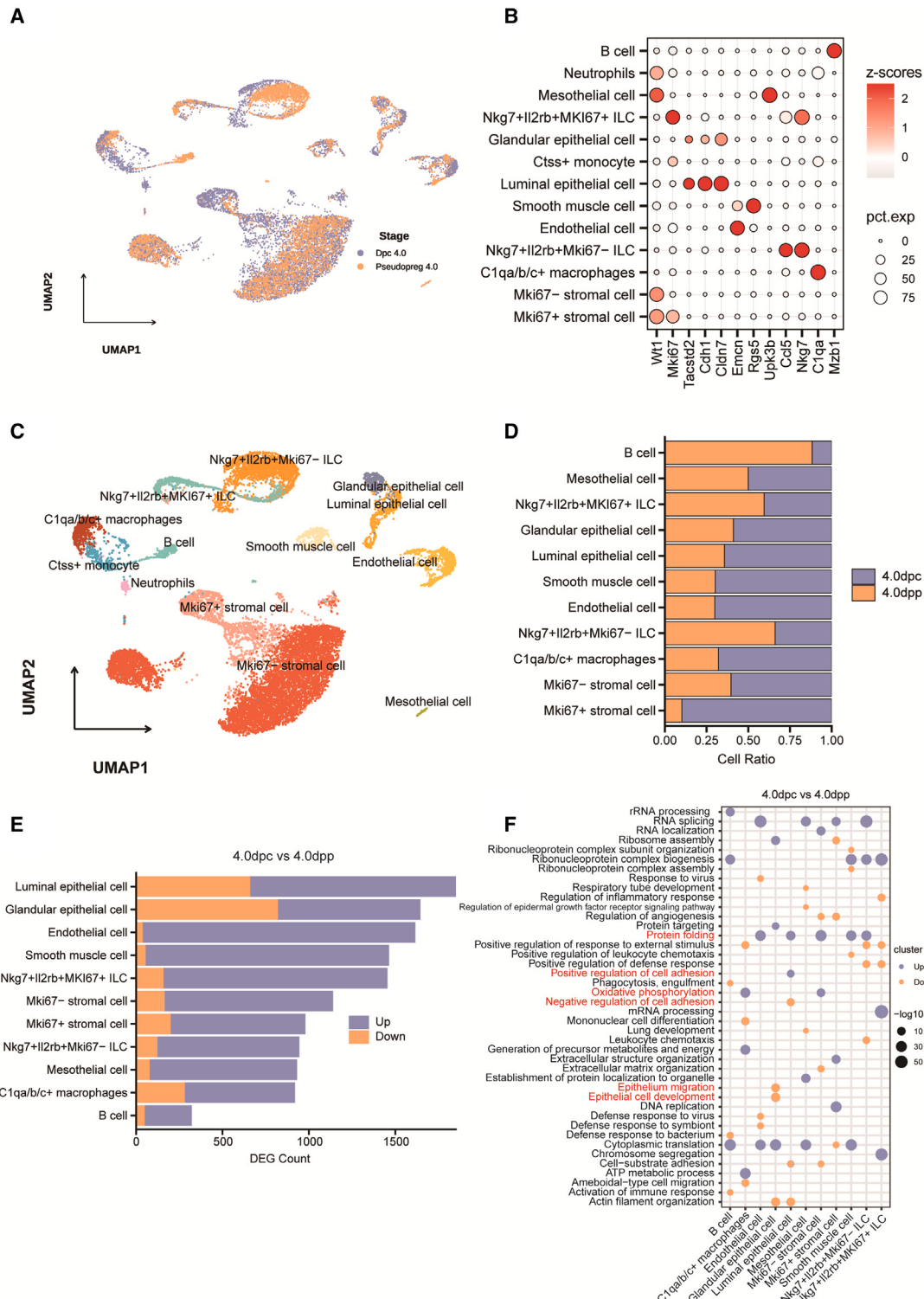


Figure 1. Endometrial luminal epithelial cells show dramatic transcriptomic changes during embryo implantation

- (A) Uniform manifold approximation and projection (UMAP) projections of scRNA-seq data from mouse uteruses at 4.0 DPC and 4.0 DPP.
- (B) Dot plot showing \log_2 -transformed expression of marker genes to identify cell types of mouse uteruses at 4.0 DPC and 4.0 DPP.
- (C) UMAP showing cell types of mouse uteruses at 4.0 DPC and 4.0 DPP.
- (D) Bar plot showing the relative proportion of cells in the mouse uteruses at 4.0 DPC and 4.0 DPP.
- (E) Bar plot showing the count of differentially expressed genes in the uteri cell population between mouse uteruses at 4.0 DPC and 4.0 DPP.
- (F) Dot plot showing the GO terms that were upregulated/downregulated in uteri cells between 4.0 DPP and 4.0 DPC.

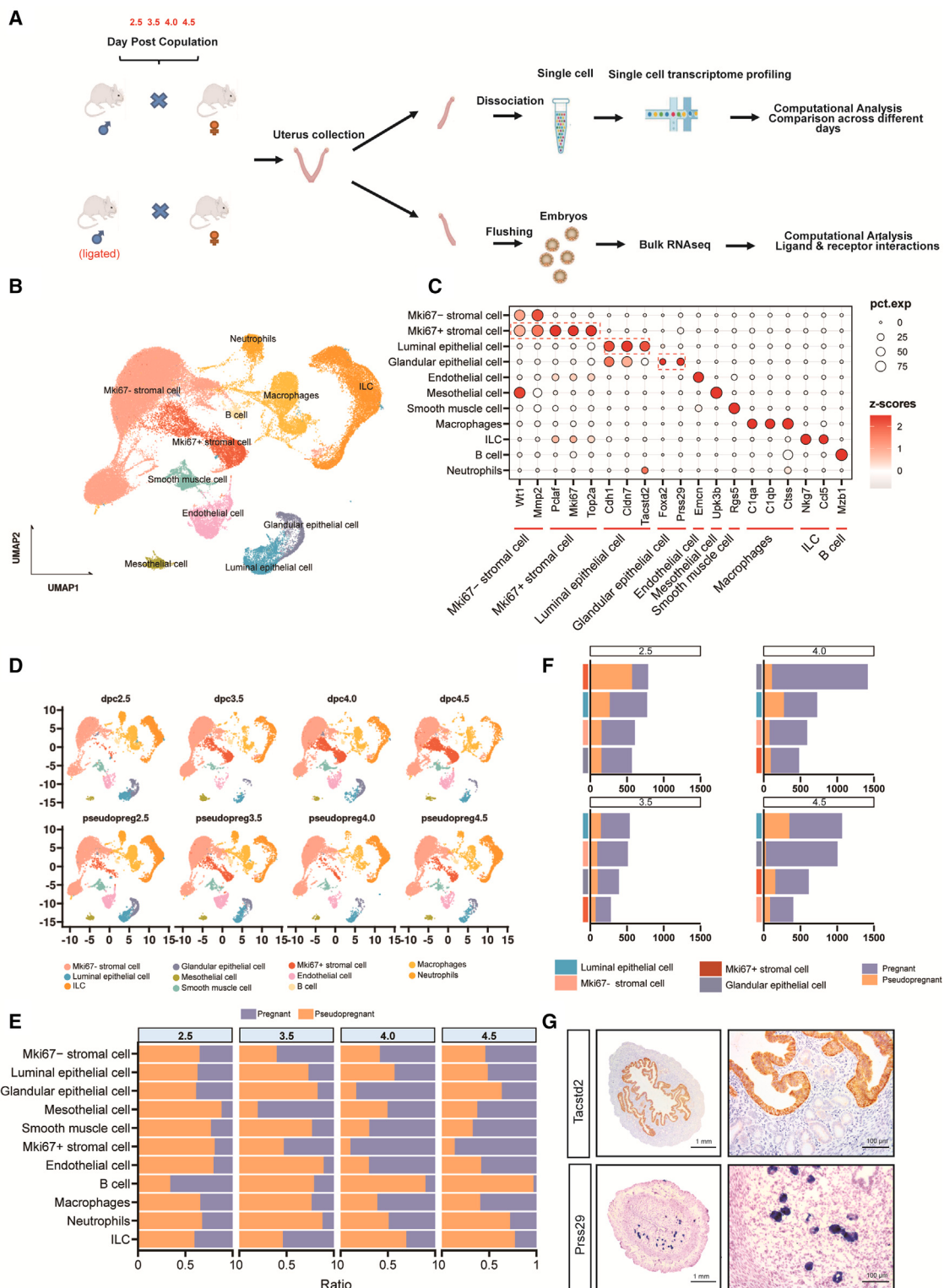


Figure 2. Single-cell profiling of the mouse uterus in pregnancy and pseudopregnancy

(A) Overview of the experimental design yielding scRNA-seq and bulk RNA-seq data from pregnant or pseudopregnant mice.
 (B) UMAP projections of scRNA-seq data from the pregnant and pseudopregnant mouse uteruses.
 (C) Dot plot showing log₂-transformed expression of marker genes to identify cell types in the mouse uteruses.

(legend continued on next page)

Developmental Cell

Resource



Luminal epithelial cells functionally differentiate into adhesive epithelial cells and SECs in the peri-implantation period

To further explore the dynamic changes in luminal epithelial cells, we isolated them by *Tacstd2* and conducted a pseudotime analysis. The analysis revealed that luminal epithelial cells differentiated across pseudotime, from “root” cells at the start of pseudotime, into two bifurcated subtypes, “branch1” and “branch2” (Figures 3A and S1A). The root cells were the main cells at 2.5 DPC, with branch1 and branch2 cells emerging at 2.5 DPC, suggesting that the differentiation of luminal epithelial cells was initiated at 2.5 DPC. The root cells almost completely disappeared, having differentiated into the two branches at 3.5 DPC. We observed a similar pseudotime trajectory in the pseudopregnant uteri (Figure S1B). The Pearson correlation coefficients of the three subtypes of luminal epithelial cells in the pregnant and pseudopregnant uteri revealed significant similarity in transcriptome features ($r > 0.95$) (Figure 3B), which suggested that luminal epithelial cell differentiation was driven by maternal signals rather than embryo-derived signals.

Next, we identified the specific markers *Ltf* and *Clu* for root cells, *Atp6v0d2* and *Olfm1* for branch1 cells, and *Il17rb* and *Calb1* for branch2 cells. We took these markers as a starting point to facilitate further experiments (Figure S1C). The ISH results confirmed that the root cells began to differentiate at 2.5 DPC and were completely transformed by 3.5 DPC. Branch1 and branch2 cells appeared from 2.5 to 4.5 DPC (Figures 3C and S1A). Interestingly, we found that *Il17rb* was expressed at 4.5 DPP (Figure S1E) but not at 4.5 DPC in branch2 (Figures 3C and S1E), which suggested an influence of embryos on luminal epithelial cells.

We then performed transcriptomic analysis of the three types of luminal epithelial cells. Clustering analysis of genes while fixing the order of cells revealed 6 distinct gene sets (Figure S1D). Kyoto Encyclopedia of Genes and Genomes (KEGG) analysis of the six gene sets showed that branch1 cells highly expressed genes associated with the “PI3K-Akt signaling pathway,” “focal adhesions,” and “Wnt signaling pathway,” whereas branch2 cells highly expressed genes related to “oxidative phosphorylation,” “pyruvate metabolism,” and “steroid biosynthesis.” Root cells expressed genes associated with the “cell cycle” (Figure 3D). These results were proven by the gene set variation analysis (GSVA) obtained for all three types of epithelial cells, where branch1 and branch2 showed distinct patterns of KEGG pathway scores (Figure S1F). Pseudotime-related gene expression analysis of several key markers showed that branch1 cells expressed higher levels of genes associated with intercellular adhesion (*Itgb6*, *Jam3*, and *Vcam1*) and extracellular matrix adhesion (*Fn1*), whereas branch2 cells expressed higher levels of genes related to metabolic activity (*Cox17* and *Ndufa6*) and ferroptosis (*Acs14* and *Alox15*) (Figure 3E). Based on all the analyses above and subsequent experimental confirmation (Figures 5 and 6), we assumed that branch1 cells were directly adhered by embryos; hence, we called them adhesive epithelial

cells (AECs) for the sake of succinctness. Furthermore, branch2 cells exhibited gene expression patterns indicative of metabolic support and were therefore named supporting epithelial cells (SECs).

Maternal estrogen and progestogen signals are critical for the functional differentiation of luminal epithelial cells during receptivity establishment

To further elucidate the maternal signals that induce functional differentiation of luminal epithelial cells, we constructed ovariectomized mouse models and mimicked the endocrinological states at the receptivity state by injecting estrogen and progestogen (Figure 4A). We found that the appearance of root luminal epithelial cells depended on estrogen stimulation (Figure 4A). Roots were found up to 2 days after estrogen treatment, but the other groups of cells did not appear at this time (Figure 4A). After the injection of estrogen and progesterone, the root completely disappeared, and AECs and SECs appeared on the luminal surface of the endometrium (Figure 4A). To further confirm the effect of E2 and P4 on root luminal epithelial cell differentiation, we isolated root luminal epithelial cells from mice at 2.5 DPC and allowed them to self-organize to generate endometrial organoids. The exposure of organoids with E2 followed by P4 decreased the expression of *Ltf* while increasing the expression of both *Olfm1* and *Il17rb*, similar to the situation *in vivo* (Figure 4B). These results indicated that the functional differentiation of AECs and SECs depended on stimulation by progesterone. Thus, the sequential stimulation of the maternal factors estrogen and progestogen was critical for the functional differentiation of luminal epithelial cells during peri-implantation. Root luminal epithelial cells expressed *Esr1*, which encodes estrogen receptors (Figure 4D, left) and was activated by estrogen (Figure 4A); hence, we called them estrogen-responsive epithelial cells (EECs).

To determine the effect of progesterone on the functional differentiation of luminal epithelial cells, we constructed transcription factor (TF) subnetworks or “regulons” using the algorithm named single-cell regulatory network inference and clustering (SCENIC) for three types of epithelial cells. Based on pseudotime order, we found that sequential regulon activation in different epithelial cells followed distinct patterns (Figure 4C, I–VIII). Notably, regulons such as *Elf3* and *Klf5* were activated in EECs and were subsequently deactivated during differentiation (Figure 4C, II), whereas *Etv6* and *Myc* continued to be activated until differentiation was complete (Figure 4C, I). In AECs, regulons such as *Twist1* and *Wt1* were activated, and both are related to the epithelial-mesenchymal transition (EMT) (Figure 4C, V). In SECs, *Klf4* was activated first (Figure 4C, VII), followed by *Gata2* (Figure 4C, VIII). *Klf4* can increase the level of oxidative phosphorylation, indicating that *Klf4* may be an important TF for enhancing the SEC metabolism rate.¹⁵ Then, we found that all three types of epithelial cells expressed *Pgr*, a gene that encodes progesterone receptor (PR) (Figure 4D, right). To further reveal the mechanism of epithelial differentiation affected by progesterone, we integrated SCENIC results with chromatin

(D) UMAP of cells from each mouse uterus to check the batch effect.

(E) Bar plot showing the relative proportion of cells in pregnant and pseudopregnant mice at each time point.

(F) Bar plot showing the count of DEGs between pregnant and pseudopregnant mice at each time point.

(G) Immunohistochemistry of TACSTD2 and *In situ* hybridization of *Prss29* expressed in the uteri of mice. Scale bars: 1 mm and 100 μ m.

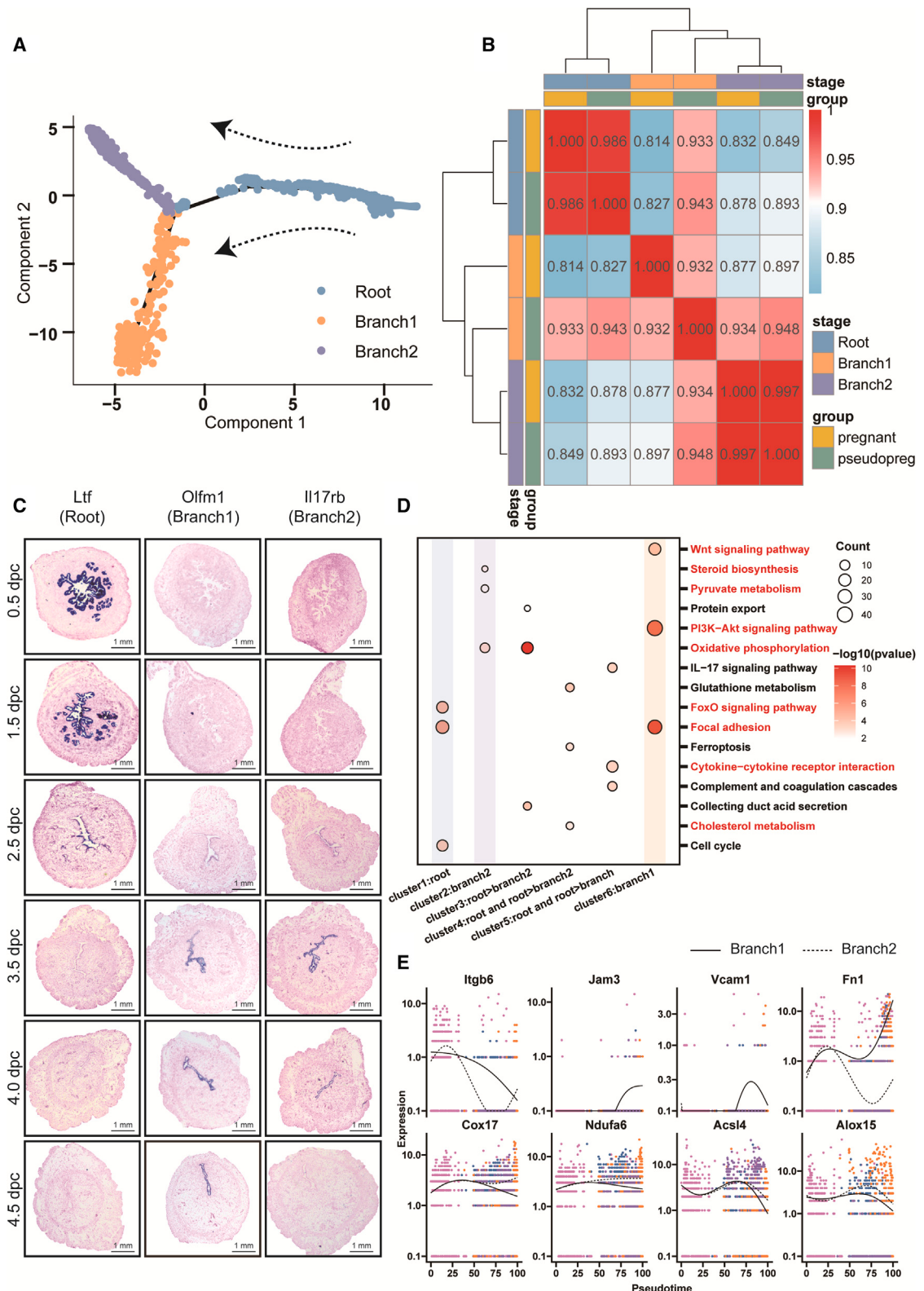


Figure 3. Functional differentiation of luminal epithelial cells during receptivity establishment

(A) Developmental pseudotime of endometrial luminal epithelial cells in pregnant mice. Arrows indicate the developmental order of these cells.
 (B) Heatmap showing the Pearson correlation coefficient of the transcriptome of three types of endometrial luminal epithelial cells between pregnant and pseudopregnant mice.

(legend continued on next page)

immunoprecipitation sequencing (ChIP-seq) results from the GEO:GSE34927 dataset, which has performed a genome-wide PR interaction site analysis based on mouse uteri treated with P4 or oil. We found that 13 TFs in EECs, 5 TFs in AECs, and 8 TFs in SECs were bound by PR (Figure 4E). We then constructed a regulatory network with the TFs in all three epithelial cell types and found that the key TFs *Fosl2* for EECs, *Ebf1* for AECs, and *Fos* for SECs might be important for the function of all three types of epithelial cells (Figures 4F and S2A). KEGG enrichment analysis confirmed the function of the target genes of these TFs, which were aligned with AEC and SEC functions: the downstream genes of *Fosl2* were involved in focal adhesion, tight junctions, and ECM-receptor interactions; the target genes of *Ebf1* were involved in the phosphatidylinositol 3-kinase (PI3K)-Akt signaling pathway, ECM-receptor interactions, and focal adhesion, and *Fos* was related to the mitogen-activated protein kinase (MAPK), WNT, and transforming growth factor β (TGF- β) signaling pathways (Figure 4G). These results suggested that progesterone might direct EEC differentiation through PR by activating TF in luminal epithelial cells.

Embryo-derived PDGF signaling regulates AEC activity and mediates embryo-endometrial interactions during implantation

Next, we compared the transcriptome profiles of AECs at 3.5, 4.0, and 4.5 DPC with those of their pseudopregnant counterparts, and we found the number of DEGs was significantly enhanced at 4.0 DPC, when embryos began to implant in uteri, compared with the number counted at 3.5 or 4.5 DPC (Figure 5A). This finding suggested that embryo-derived signals induced changes in the transcriptome in AECs, which might be important to establish receptivity and ensure embryo implantation. To investigate this communication between the embryo and uterus, we collected the embryos on the other side of the uterus and performed RNA-seq (Figure 1A). We found that the transcriptome of the embryos at 4.0 DPC significantly differed from that at 3.5 DPC (Figures S3A and S3B). GO and KEGG analyses of DEGs showed that cell-substrate adhesion, cell junction assembly in GO and focal adhesion, and the TGF- β signaling pathway in KEGG were upregulated at 4.0 DPC compared with those at 3.5 DPC (Figures S3C and S3D). Next, we leveraged a single-cell dataset of embryos that have undergone lineage specialization to evaluate the expression of these genes in the subpopulation of embryos.¹⁶ Additionally, we found that in all upregulated genes related to cell-substrate adhesion in embryos at 4.0 DPC, 46.0% genes specifically expressed in trophectoderm (TE) (Figures S3E). These results suggested that it might be TE-derived signals to mediate the communication between embryo and luminal epithelium. Then, we used bulk and scRNA-seq data from both embryo and uterus at all time points (for embryos, bulk data at 3.5 and 4.0 DPC and published scRNA-seq data at 4.5 DPC¹⁶) to identify ligand-receptor pairs in which the ligands

were from embryos and the receptors were from AECs using the CellChat package. To separate embryo-derived signals from maternal signals, we removed receptors that were expressed in pseudopregnant mice and receptors whose expression did not differ from that in pregnant mice. The remaining ligand-receptor pairs, which we called embryo-to-AEC LRs, were assumed to be secreted from the embryo and bind to AECs. Using this strategy, we identified 31 LR pathways (Figure 5B), among which the WNT, EGF, and SPP1 signaling pathways have been reported to mediate embryo-endometrium crosstalk, whereas the EPHB, PDGF, and PROS signaling pathways have not been previously reported. To investigate the impact of embryo-derived signaling on AECs, we considered DEGs between pregnant and pseudopregnant mice at each time point as potential embryo ligand-targeted genes. Then, we predicted the regulatory relationships between embryo-to-AEC LRs and embryo ligand-targeted genes using the nichenetR package. We identified 16 ligands from 31 LR pairs (Figure 5C), including WNT7B and WNT4, which were expressed in the TE and have been previously reported, as well as PDGFA, which was also expressed in TE but had not been previously studied (Figures 5C and S3F). Moreover, GO enrichment analysis revealed that the embryo ligand-targeted genes were mainly involved in epithelial cell remodeling, including morphogenesis of branching epithelial cells and epithelial cell migration and adhesion, including ECM organization and the positive regulation of cell adhesion (Figure 5D), which suggested embryo-derived signaling regulates adhesion between embryos and AECs. Next, we injected the PDGFR antagonist imatinib into one side of the uterus and normal saline into the other side as a control at 2.5 DPC; we then transferred the embryos into mice. We found that the number of embryo implantation sites on the imatinib-treated side of uteri was significantly reduced at 4.5 DPC, suggesting that the PDGF pathway plays a vital role in embryo implantation (Figures 5E and 5F; Table S1). Hematoxylin and eosin (H&E) staining of the implanted embryos indicated that embryonic development was not affected by PDGF inhibition (Figure 5G), although embryo implantation was inhibited. Based on another AEC marker at 4.5 DPC, *Nudt19*, we found that AECs at 4.5 DPC were only near the implantation site (Figure 5H). Additionally, we found that the litter size was lower in the group treated with imatinib than in the normal saline group at 18.5 DPC ($p < 0.05$), but there were no significant differences in the weight of pups between these two groups ($p > 0.05$) (Figure 5I).

Embryo-derived Efna/EPHA signaling regulates SEC activities and affects the formation of the primary decidual zone

Next, we compared the transcriptome profile of the SECs from 3.5 to 4.5 DPC with that of their pseudopregnant counterparts. The analysis revealed a significant increase in the number of

(C) *In situ* hybridization markers of luminal Root (*Ltf*), branch1 (*Olfm1*), and branch2 (*Il17rb*) in the mouse uteruses at 0.5–4.5 DPC. Scale bars: 1 mm.

(D) Dot plot showing KEGG enrichment results of clusters of genes that are differentially expressed across pseudotime. Labels of hierarchical axis were according to cluster name from Figure S1D. Point size represents the number of genes enriched in the pathways. The color bar represents $-\log_{10}$ -transformed p values of the pathways.

(E) Expression levels (vertical axis) of key genes between branch1 and branch2 ordered in pseudotime (cell colors were according to time points from Figure S2A). See also Figure S1.

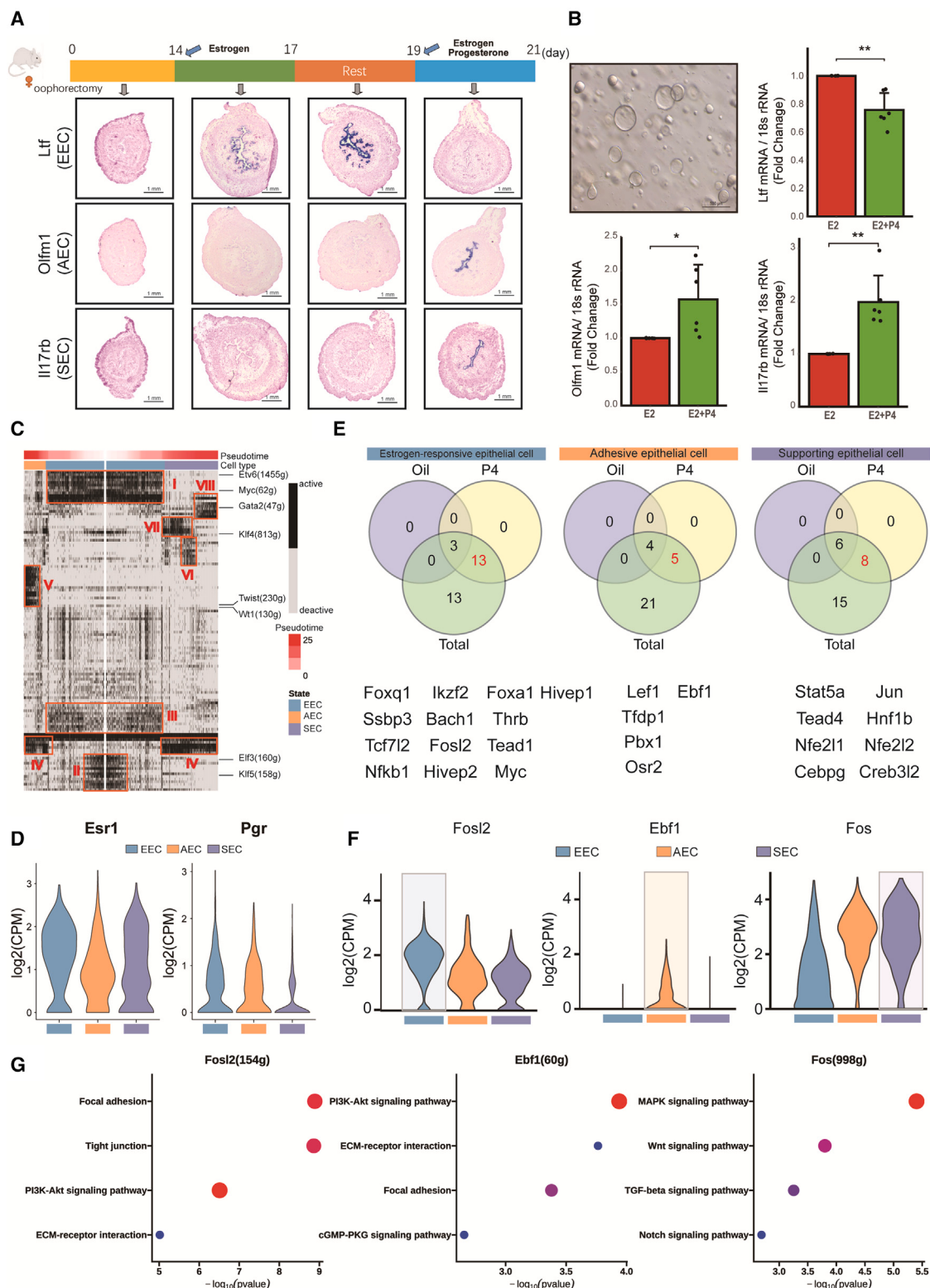


Figure 4. Functional differentiation of luminal epithelial cells is induced by maternal signals

(A) Model diagram of hormone model mouse uterine sample collection and *in situ* hybridization markers of estrogen-responsive epithelial cells (*Ltf*), adhesive epithelial cells (*Olfm1*), and supporting epithelial cells (*Il17rb*) in the mouse uteruses. Scale bars: 1 mm.

(B) Image of organoids from Root luminal epithelial cells in expansion medium and real-time qPCR analysis for markers of estrogen-responsive epithelial cells (*Ltf*), adhesive epithelial cells (*Olfm1*), and supporting epithelial cells (*Il17rb*). Scale bars: 500 μ m. Data represent the means \pm SD. * $p < 0.05$; ** $p < 0.01$.

(legend continued on next page)

DEGs at both 4.0 and 4.5 DPC, which corresponded to the period of embryo implantation and the subsequent stages (Figure 6A). Using the same strategy, we identified 15 LR pairs whose ligands were expressed by embryos and receptors were expressed by SECs at 4.0 and 4.5 DPC (Figure 6B). Among them, the receptors of WNT, EPHB, SPP1, VISFATIN, COLLAGEN, and LAMNIN were also found in AECs, whereas the receptors of BMP, fibroblast growth factor (FGF), and EPHA were SEC-specific. Then, we identified 6 ligands produced by E4.0 embryos and 9 ligands produced by E4.5 embryos and predicted the interactions between ligands and embryo-related DEGs in SECs using the nichenetR package (Figure 6C). Notably, the ligands included *Lamc2* and *Lamb1*, as well as *Efna3* and *Efna4*, which were expressed in TE (Figure S3G) but had not been previously reported. GO enrichment analysis revealed that these regulated genes were involved in protein phosphorylation, regulation of apoptotic signaling pathways, and positive regulation of catabolic processes at both 4.0 and 4.5 DPC (Figure 6D). For verification, the *EphA1* (receptor for *Efna3* and *Efna4*) small interfering RNA (siRNA) mixture was injected into one side of the uterus to knock down its expression, and control siRNA was injected on the other side at 2.5 DPC. Then, both sides were transferred with the same number of embryos. We found that the number of embryo implantation sites in the *EphA1* siRNA-treated uterus was significantly reduced at 4.5 DPC, suggesting that the *EphA1* pathway plays a critical role in embryo implantation (Figures 6E and 6F; Table S1). HE examination of the implanted embryos indicated that embryonic development was not affected by *EphA1* knockdown, but the area of PDZ was decreased, and decidualization-related genes *Prl8a2* and *Foxo1* were both significantly decreased after *EphA1* knockdown (Figures 6G and 6H). The results suggested that communications between embryos and SECs were related to PDZ formation, which further affects embryo implantation.

Both luminal epithelial cell differentiation and communication between the fetus and mother are conserved in humans and mice

Four groups of epithelial cells are included in the human endometrium: glandular epithelial cells, unciliated luminal epithelial cells, ciliated luminal epithelial cells, and SOX9-positive luminal epithelial cells.¹² Using the GEO:GSE111976 dataset, we mapped out the trajectory of the differentiation of human luminal epithelial cells, and we found that SOX9-positive epithelial cells differentiated into two groups, unciliated luminal epithelial cells, and ciliated luminal epithelial cells, from the proliferative stage to the secretory stage, similar to what happens in the mice in which EECs differentiated into AECs and SECs at 2.5 DPC (Figure S4A). Therefore, we compared our dataset with the human endome-

trium GEO:GSE111976 dataset.¹² To determine the endometrial luminal epithelial cell similarity of mice and humans, we used the algorithm named single-sample gene set enrichment analysis (ssGSEA) to calculate DEG activity among the three types of epithelial cells in both mice and humans after transforming the mouse DEGs into homologous human genes (detailed in STAR Methods section). We found that human SOX9-positive epithelial cells were similar to mouse EECs, whereas human ciliated epithelial cells were similar to mouse AECs, and human unciliated epithelial cells were similar to mouse SECs (Figures 7A and 7B). These results suggested conserved differentiation processes of endometrial luminal epithelial cells in humans and that they are similar to those in mice.

As we did with the mouse data, we also analyzed signaling crosstalk between the endometrium and embryo in humans using CellChat and two human datasets, GEO:GSE109555 for the embryo and GEO: GSE111976 for the endometrium samples. To identify the signaling coming specifically from the embryo, we isolated cells from blastocysts at D6 (pre-implantation) and D8 (post-implantation) to track communication from the embryo to the luminal epithelium of the endometrium at the mid-secretory phase. In the end, we identified a total of 55 LR pairs, including previously reported FN1 and LAMA1. We also found LR pairs in the EPHA pathway in humans (Figure S4B). We also determined in which layers of blastocysts these embryo-derived ligands were expressed. For example, we found that EFNA4, a ligand in the EPHA pathway, was expressed in EPs, whereas EFNA1 was expressed in TEs (Figure S4C), which was not seen in mice. By analyzing the conserved communication between embryos and uteri in humans and mice, we found signaling from embryos to ciliated luminal epithelial cells of 16 conserved LRs (34.8% in humans) that were involved in 10 pathways (66.7% in humans) and signaling from embryos to unciliated luminal epithelial cells of 11 conserved LRs (20% in humans) that were involved in 8 pathways (50% in humans) (Figure 7C). The LR pairs showed less species conservation than the pathways. These results indicated that in addition to endometrial luminal epithelial cell differentiation, maternal-embryonic communications were similar between humans and mice.

Defective differentiation and function of luminal epithelial cells may contribute to a thin endometrium and RIF

To explore the clinical relevance of epithelial cell differentiation during peri-implantation, we selected two types of endometrial diseases, thin endometrium and RIF. We used Scissor algorithm to integrate single-cell data with bulk sequence datasets to predict pathology-related cell population alterations in the endometrium.

(C) Heatmap showing the activities of regulons in luminal epithelial cells according to SCENIC analysis. Black represents the active status of regulons, and gray represents the inactive status of regulons.

(D) Violin plot showing log₂-transformed expression of *Esr1* and *Pgr* in three types of luminal epithelial cells.

(E) Venn diagram showing the relationship between TFs filtered from oil-treated and P4-treated mouse uteruses and regulons derived from SCENIC analysis. Oil represents TFs filtered from oil-treated mouse uteri. P4 represents TFs filtered from progesterone-treated mouse uteri. Total represented regulons (TFs) derived from SCENIC analysis.

(F) Violin plot showing log₂-transformed expression of key TFs in three types of luminal epithelial cells.

(G) Dot plot showing KEGG enrichment results of target genes regulated by key TFs.

See also Figure S2.

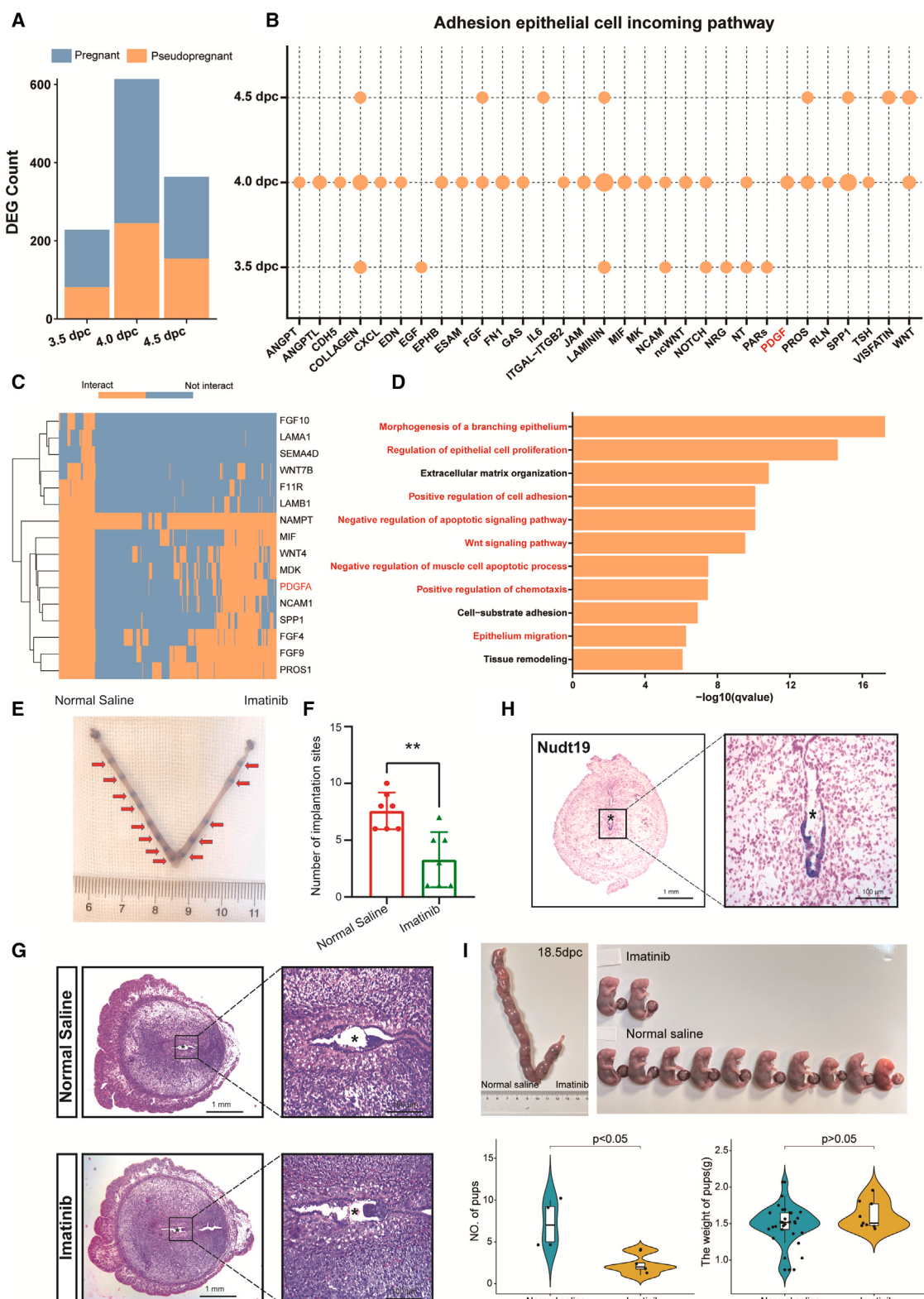


Figure 5. Embryo-derived signals regulate AEC activity and implantation

(A) Bar plot showing the number of DEGs in AECs between pregnant and pseudopregnant mice.
(B) Dot plot showing the embryo-derived signals interacted with AECs at the pathway level.

(legend continued on next page)

Developmental Cell Resource



For thin endometrium, using Scissor, we integrated our thin endometrium bulk sequence data with our previously published single-cell data of thin endometrium¹⁸ (Figures S5A and S5C). This identified 1,120 Scissor (-) cells and 580 Scissor (+) cells in the single-cell dataset (Figures 7D and S5B). Scissor (+) cells comprised a cell population associated with the thin endometrium, Scissor (-) cells comprised a cell population associated with the normal endometrium, and the other cells were background cells and considered unrelated to this phenotype. We found that both Scissor (+) and Scissor (-) cells were abundantly distributed in the stromal cell population (Figure S5D), which was consistent with the proliferation and widespread distribution of stromal cells during the proliferative phase in the endometrium. Interestingly, epithelial cells were the second most abundant cell type (Figure S5D), with both Scissor (+) and Scissor (-) cells distributed in SOX9-positive epithelial cell populations (Figure 7D). The comparison of the transcriptome between Scissor (+) and Scissor (-) SOX9-positive epithelial cells confirmed that processes associated with the negative regulation of the WNT signaling pathway were upregulated, whereas those associated with positive regulation of the NOTCH signaling pathway were downregulated in Scissor (+) SOX9-positive epithelial cells (Figure 7F). Notably, activation of the WNT and NOTCH signaling pathways in the differentiation of secretory luminal and glandular epithelial cells in the endometrium had already been proven by Garcia-Alonso et al. These results suggested that the dysfunction of SOX9-positive epithelial cells was related to thin endometrium. To verify the results described above, we detected the expression of β -catenin in the normal and thin endometrium groups in the proliferative phase using immunofluorescence and found that β -catenin expression in the luminal epithelium of the thin endometrium was significantly lower than that of the normal group (Figure S5E), indicating that the WNT signal in the luminal epithelium of the thin endometrium was indeed weaker than that of the normal group.

For RIF, we performed scRNA-seq on three patients. This yielded 7 major groups of cells based on their marker expression: (1) glandular epithelial cells (PAEP), (2) ciliated epithelial cells (PIFO), (3) unciliated luminal cells (PTGS1 and PAX2), (4) stromal cells (insulin growth factor 1[IGF1]), (5) endothelial cells (CD34), (6) lymphoid cells (PTPRC), and (7) myofibroblasts (ACTA2) (Figures 7E and S6A). To identify cell populations associated with RIF, we integrated our data with bulk RNA-seq data obtained from the GEO:GSE26787 database¹⁹ using Scissor. We obtained 154 Scissor (+) cells associated with RIF and 336 Scissor (-) cells associated with the control (Figure 7E). Interestingly, we found that Scissor (+) cells were distributed in the luminal un-

ciliated epithelial cell population (Figure 7E). Compared with Scissor (-) cells, we found that processes related to metabolism, such as acyl-coenzyme A (CoA) biosynthetic process, sterol biosynthetic process, and fatty acid beta-oxidation, were upregulated in Scissor (+) cells (normalized enrichment score [NES] > 0), whereas cellular response to copper ion, positive regulation of cell killing and type I interferon signaling pathway were downregulated in Scissor (+) cells (NES < 0) (Figure 7G). To verify the results described above, we checked the expression of CYP26A1, IDH1, SQLE, and XDH, which were related to sterol and fructose metabolism and were upregulated in Scissor (+) cells, in unciliated luminal epithelial cells and two datasets (GEO:GSE26787 and GEO:GSE92324),²⁰ and we found that all four genes were not only highly expressed in Scissor (+) cells (Figure S6B) but were significantly higher in the endometrium of RIF than in the endometrium of the normal group (Figure S6C), indicating abnormal metabolic function of the unciliated luminal epithelium in RIF patients.

In conclusion, our results revealed that the impaired differentiation and functions of the luminal epithelium could contribute to thin endometrium and RIF.

DISCUSSION

Embryo implantation requires comprehensive maternal-fetal dialog, but the temporal and cell-specific coordination of this communication is largely unknown because of the cellular complexity and dynamic developmental processes of both the embryo and endometrium during peri-implantation. In this article, we constructed a cell census to describe the dynamics of the whole uterus during peri-implantation.

During receptivity establishment, the hormone-induced switch in endometrial cell activity is an indicator that the uterus is ready for implantation of an embryo entering the uterus.²¹⁻²³ Garcia-Alonso et al.¹⁷ reported that the human epithelium in the secretory phase could be divided into secretory epithelium (glandular) and ciliated epithelium (luminal), but the functional differentiation of luminal epithelial cells caused by hormones has not been reported. In this study, we found that at 2.5 DPC, a group of EECs was generated by estrogen stimulation in the mouse endometrium, and then, these epithelial cells differentiated into two groups of functional cells, AECs and SECs, in response to progesterone but not embryo-derived signaling. It has been reported that mice with *Pgr* specifically knocked out in uterine epithelial cells showed defective epithelial cell proliferation and embryo adhesion failure.²⁴ We have shown that progesterone regulates the differentiation of the uterine epithelium by

(C) Heatmap showing DEGs of AECs between pregnant and pseudopregnant mouse uteri targeted by embryo-derived signals. The x axis represents the DEGs between the pregnant and pseudopregnant groups, which were considered potential embryo ligand-targeted genes. "Interact" means that the signals could potentially regulate the target genes, and "not interact" means that the signals could not potentially regulate the target genes.

(D) Bar plot showing enriched GO terms of gene targets by embryo-derived signals.

(E) Representative uteri treated with normal saline or the PDGF inhibitor imatinib on 4.5 DPC (n = 6).

(F) Number of embryo implantation sites treated with normal saline or the PDGF inhibitor imatinib on 4.5 DPC (n = 6). Data are represented as mean \pm SD.

** p < 0.01.

(G) Hematoxylin and eosin staining of implantation sites treated with normal saline or the PDGF inhibitor imatinib on 4.5 DPC. Scale bars: 1 mm and 100 μ m.

(H) *In situ* hybridization markers of adhesive epithelial cells (*Nudt19*) in the uteri of mice on 4.5 DPC. Scale bars: 1 mm and 100 μ m.

(I) Representative uteri treated with normal saline or the PDGF inhibitor imatinib on 18.5 DPC, violin plot showing the number of pups obtained from these two groups and the weight of these pups.

See also Figure S3.

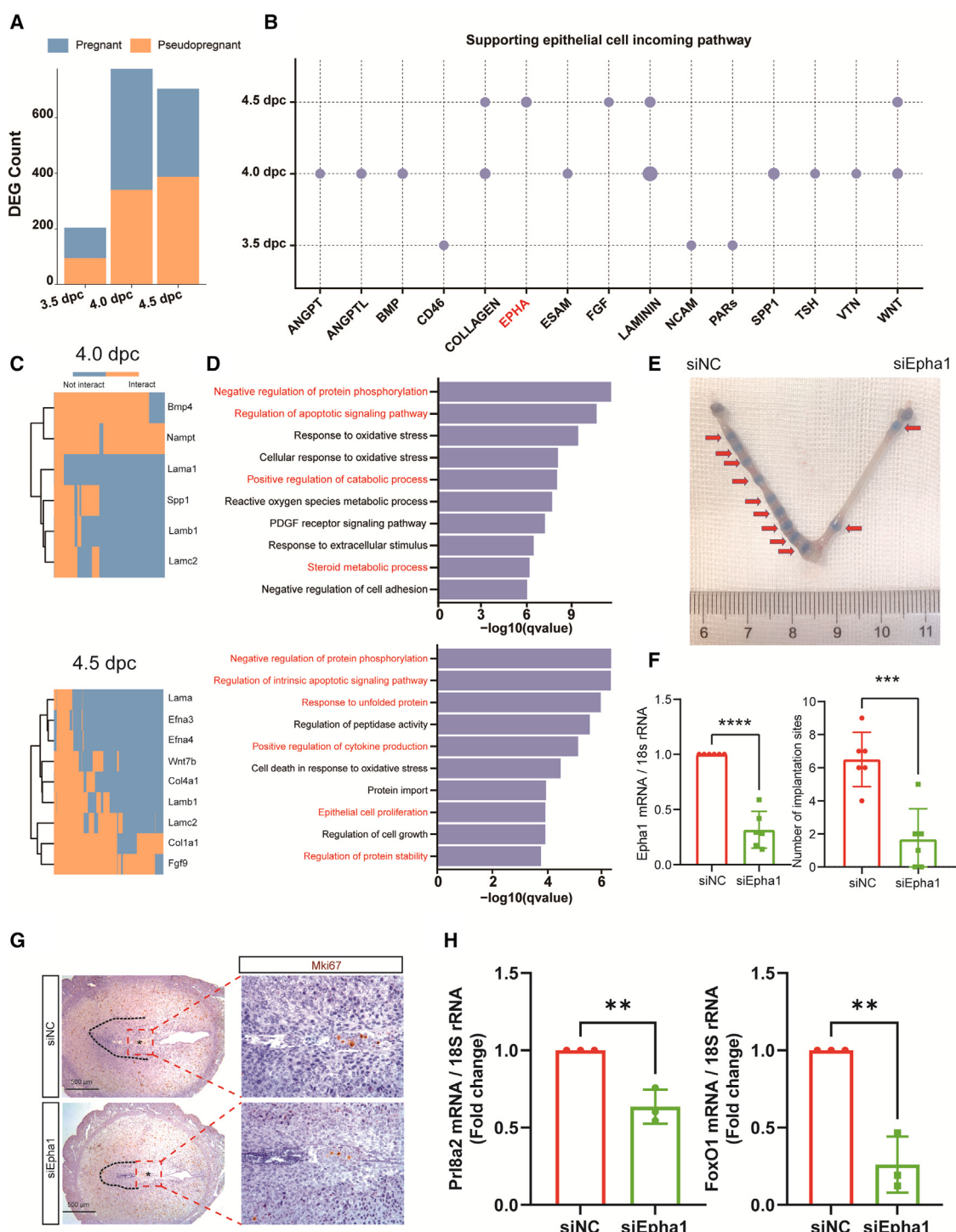


Figure 6. Embryo-derived signals regulated SEC activity and implantation

- (A) Bar plot showing the number of DEGs in the SEC between pregnant and pseudopregnant mice.
- (B) Dot plot showing the embryo-derived signals interacted with the SEC at the pathway level.
- (C) Heatmap showing DEGs of the SEC between pregnant and pseudopregnant mouse uteri targeted by embryo-derived signals at 4.0 and 4.5 DPC. The x axis represents the DEGs between the pregnant and pseudopregnant groups, which are considered potential embryo ligand-targeted genes. Interact means that the signals could potentially regulate the target genes, and "not interact" means that the signals could not potentially regulate the target genes.
- (D) Bar plot showing enriched GO terms of gene targets by embryo-derived signals at 4.0 and 4.5 DPC.
- (E) Representative uteri treated with NC siRNA or *EphA1* siRNA mixture on 4.5 DPC (n = 6).

(legend continued on next page)

activating many TFs in uterine luminal epithelial cells, mediated by Pgr; these TFs include *Twist1* in AECs and *Fosl2* in EECs, which control switching between uterine epithelial cell proliferation and differentiation and affect uterine receptivity.^{25–28}

Embryo implantation is a critical event that relies on proper maternal-embryonic crosstalk. Considering the aforementioned results, we found that changes in the transcriptome in the mouse AECs at 4.0 DPC were more dramatic than those in mice on day 4.0 of pseudopregnancy, which indicated that AEC activity was specifically regulated by embryo-derived signaling but not maternal signaling. Because we were limited to bulk RNA-seq data of the endometrium obtained in previous studies, it was difficult to precisely determine the crosstalk of the embryo and uterus. In our study, we resolved many signals transmitted from the embryo to AECs and SECs, such as WNT, SPP1, PDGF, and EPHA signals, at single-cell resolution. Dkk1 mediates the inhibition of WNT/β-catenin signaling, which has no negative effect on mouse uterine receptivity but significantly inhibits embryo adhesion.²⁹ Moreover, SPP1 signaling promotes embryo adhesion by binding ITGAV.³⁰ In the present study, we established a more systematic and comprehensive regulatory network of embryo-derived signaling, especially signaling in two luminal epithelial cell subpopulations: AECs and SECs. Furthermore, we found that the functional effects of these signaling pathways on AECs and SECs were related to epithelial cell remodeling processes and protein phosphorylation, respectively, which may be consistent with the adhesion function of AECs and the nutritional and supportive function of SECs. Furthermore, we demonstrate the promotion of embryo implantation by the key embryo-derived signaling of *Pdgfa* and *Efna3/4*. According to previously obtained transcriptome data from trophoblast cells and endometrial cells during embryo implantation, *Pdgfa* expression was upregulated in human trophoblast cells, and its corresponding receptor, *Pdgfra*, was overexpressed in the endometrium of pregnant women,⁸ suggesting that PDGF signaling is involved in the early dialog between blastocysts and maternal endometrial cells. On the other hand, *Epha1* was mainly expressed in mouse endometrial epithelial cells, whereas its ligand ephrin A1–4 was expressed in blastocysts.³¹ In our results, the inhibition of PDGF signaling significantly reduced embryo implantation efficiency. Similarly, after we knock downed *Epha1* in the uterus, the embryo implantation efficiency also decreased significantly. These results indicated that PDGF and EPHA signaling in the embryo acted on the luminal epithelium, playing an important role in embryo implantation.

Recently, intrauterine infusion of autologous platelet-rich plasma (PRP) has been used in clinical practice for the treatment of thin endometrium and RIF.^{32,33} PRP releases numerous cytokines, growth factors, and chemokines stored in the alpha granules of platelets, and these molecules promote tissue regeneration. For instance, platelet-derived IGF1 and SDF-1α play important roles in cell differentiation.^{34,35} Thus, we suggest that one of the potential reasons for the improvement of clinical

outcomes of thin endometrium and RIF patients who received PRP treatment might be that PRP facilitates endometrial luminal epithelium differentiation. Growing evidence has revealed metabolic disorders in the RIF patient endometrium,^{36,37} which partially confirms our scRNA-seq results and provides new insights into the pathogenesis of RIF and the search for more efficient treatments.

In conclusion, our results reveal the dynamics and molecular mechanisms of the epithelium during the establishment of receptivity and embryo implantation under the regulation of maternal and embryonic signaling. We also provide a reference for understanding the cytological behavior during the establishment of endometrial receptivity. Specifically, by determining the degree of conservation of epithelial cell differentiation and maternal-embryo communication in humans and mice, we demonstrated the association of impaired epithelial cells with endometrial function in thin endometrium and RIF.

Limitations of the study

However, there are also some limitations of our study on the pathogenic mechanisms of thin endometrium and RIF. Although epithelial cells appear to play an important role, stromal and immune factors are also considered to be important. For instance, our single-cell dataset for thin endometrium showed the highest number of Scissor (+) cells in stromal cells, followed by epithelial cells. Moreover, upon analyzing other published single-cell datasets³⁸ for RIF, it was found that patients with epithelial defects comprised only half of all patients. These findings remind us that further attention is needed in the mechanistic investigation of thin endometrium and RIF.

STAR★METHODS

Detailed methods are provided in the online version of this paper and include the following:

- **KEY RESOURCES TABLE**
- **RESOURCE AVAILABILITY**
 - Lead contact
 - Materials availability
 - Data and code availability
- **EXPERIMENTAL MODEL AND STUDY PARTICIPANT DETAILS**
 - Patients and samples
 - Mice
- **METHOD DETAILS**
 - Uterine tissue collection
 - Ovariectomy and hormone induction models
 - Bulk RNA-seq library preparation and data analysis
 - 10X Genomics library preparation, sequencing, and acquisition of an expression matrix
 - Data processing, batch effect correction and cell identification

(F) mRNA expression levels of *Epha1* in siNC and si*Epha1* groups examined by real-time qPCR ($n = 6$) and number of embryo implantation sites treated with NC siRNA and *Epha1* siRNA mixture on 4.5 DPC ($n = 6$). Data are represented as mean \pm SD. *** $p < 0.001$; **** $p < 0.0001$.

(G) Hematoxylin and eosin staining of implantation sites treated with NC siRNA or *Epha1* siRNA mixture on 4.5 DPC. Scale bars: 500 μ m.

(H) mRNA expression levels of *Prl8a2* and *Foxo1* examined by real-time qPCR in NC siRNA and *Epha1* siRNA mixture treated mouse uteruses. Data are represented as mean \pm SD. ** $p < 0.01$.

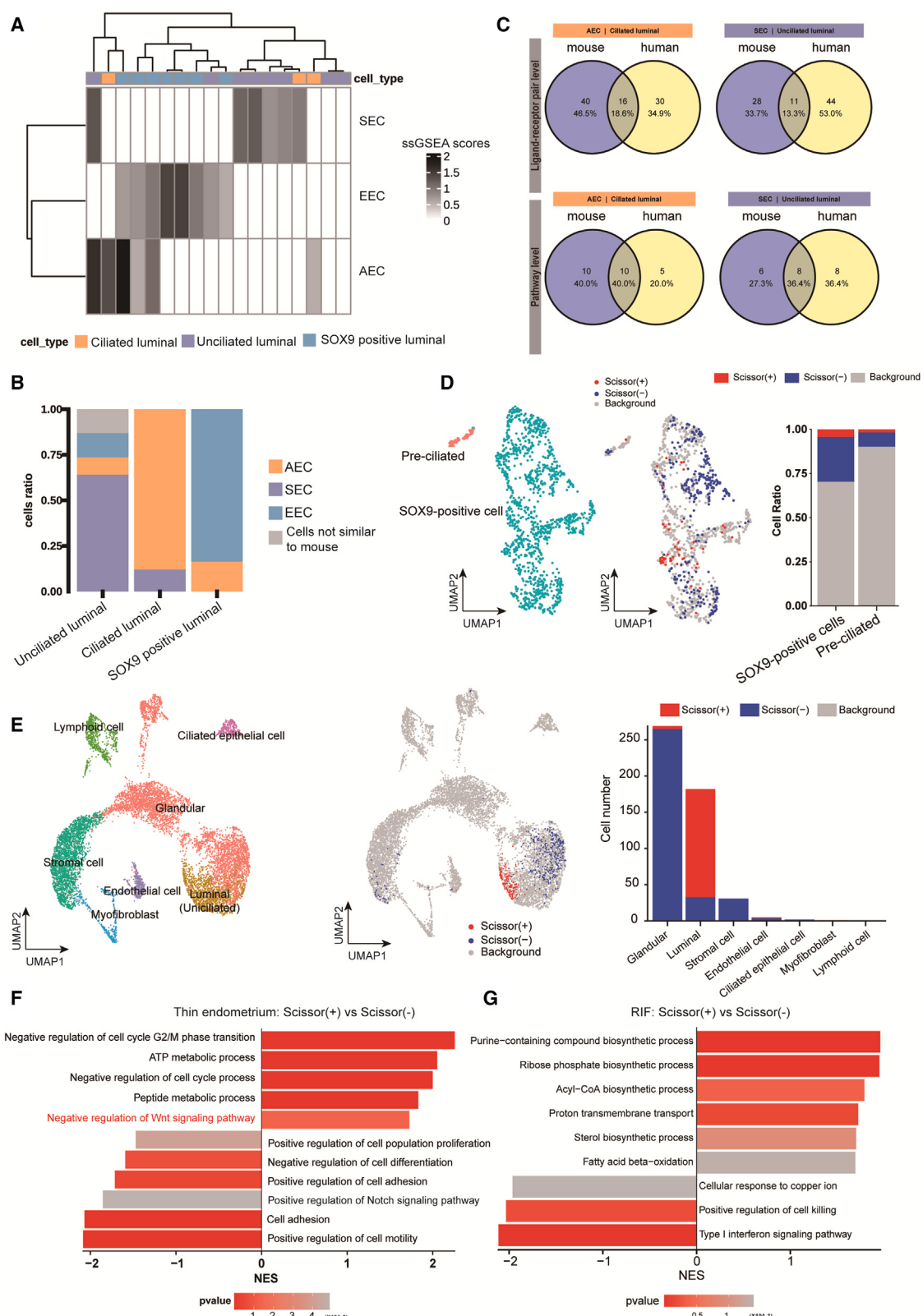


Figure 7. Both luminal epithelial cell differentiation and communication between the fetus and mother are conserved between humans and mice

(A) Heatmap showing ssGSEA scores calculated by marker genes of three types of mouse luminal epithelial cells in human luminal epithelial cells.

(legend continued on next page)

Developmental Cell Resource



- Pseudotime analysis
- Correlation analysis
- Transcription factor-related gene regulation subnet-work analysis
- Cell-cell communication analysis
- Gene enrichment analysis
- ssGSEA
- Real-time qPCR (RT-qPCR) verification
- In situ hybridization
- Immunohistochemistry staining
- Hematoxylin and eosin (H&E) staining
- Immunofluorescence
- Mouse embryo transplantation assay
- Organoid culture from mouse endometrium
- Induction differentiation of endometrial organoids

● QUANTIFICATION AND STATISTICAL ANALYSIS

SUPPLEMENTAL INFORMATION

Supplemental information can be found online at <https://doi.org/10.1016/j.devcel.2023.08.004>.

ACKNOWLEDGMENTS

This work was supported by the National Natural Science Foundation of China (82030040, 82171653, 81871165, 31872846, and 81971387). We thank OE Biotech Co., Ltd. (Shanghai, China) and LC-BIO Technologies Co., Ltd. (Hangzhou) for providing single-cell RNA-seq and bulk RNA-seq. We thank Dr. Jianming Zeng (University of Macau), and all the members of his bioinformatics team, biotrainingee, for generously sharing their experience and codes.

AUTHOR CONTRIBUTIONS

H.-X.S., G.-J.Y., C.-J.L., Z.-B.H., Y.-L.H., and L.-J.D. designed and supervised the experiments; Y.L., J.-Y.L., Y.J., Z.-L.W., and X.-Y.T. prepared clinical samples and mice; H.-Q.W., Y.-L.H., C.-F.Y., Z.-W.C., and X.-Q.S. performed computational analyses; H.-Q.W., Y.L., D.L., J.-Y.L., Y.J., X.-Y.T., Y.Z., and X.Z. performed the mouse embryo transplantation assay; H.-Q.W., Y.L., D.L., J.-Y.L., Y.J., Q.-L.Y., and J.-D.Z. performed immunohistochemistry, immunofluorescence, and ISH; H.-Q.W., Y.L., D.L., J.-Y.L., and Y.J. performed the organoid experiments; H.-X.S., G.-J.Y., C.-J.L., Y.-L.H., J.-Y.L., and Y.J. provided pathological expertise; H.-Q.W., Y.L., D.L., J.-Y.L., and Y.J. wrote the manuscript. All authors read and approved the manuscript.

DECLARATION OF INTERESTS

The authors declare no competing interests.

Received: June 20, 2022

Revised: April 11, 2023

Accepted: August 1, 2023

Published: August 28, 2023

REFERENCES

1. Carson, D.D., Bagchi, I., Dey, S.K., Enders, A.C., Fazleabas, A.T., Lessey, B.A., and Yoshihaga, K. (2000). Embryo implantation. *Dev. Biol.* 223, 217–237. <https://doi.org/10.1006/dbio.2000.9767>.
2. Wang, H., and Dey, S.K. (2006). Roadmap to embryo implantation: clues from mouse models. *Nat. Rev. Genet.* 7, 185–199. <https://doi.org/10.1038/nrg1808>.
3. Ng, S.W., Norwitz, G.A., Pavlicev, M., Tilburgs, T., Simón, C., and Norwitz, E.R. (2020). Endometrial decidualization: the primary driver of pregnancy health. *Int. J. Mol. Sci.* 21. <https://doi.org/10.3390/ijms21114092>.
4. Franco, H.L., Rubel, C.A., Large, M.J., Wetendorf, M., Fernandez-Valdivia, R., Jeong, J.W., Spencer, T.E., Behringer, R.R., Lydon, J.P., and Demayo, F.J. (2012). Epithelial progesterone receptor exhibits pleiotropic roles in uterine development and function. *FASEB J.* 26, 1218–1227. <https://doi.org/10.1096/fj.11-193334>.
5. Lessey, B.A., Ilesanmi, A.O., Lessey, M.A., Riben, M., Harris, J.E., and Chwalisz, K. (1996). Luminal and glandular endometrial epithelium express integrins differentially throughout the menstrual cycle: implications for implantation, contraception, and infertility. *Am. J. Reprod. Immunol.* 35, 195–204. <https://doi.org/10.1111/j.1600-0897.1996.tb00031.x>.
6. Genbacev, O.D., Prakobphol, A., Foulk, R.A., Krtolica, A.R., Ilic, D., Singer, M.S., Yang, Z.Q., Kiessling, L.L., Rosen, S.D., and Fisher, S.J. (2003). Trophoblast L-selectin-mediated adhesion at the maternal-fetal interface. *Science* 299, 405–408. <https://doi.org/10.1126/science.1079546>.
7. Illera, M.J., Cullinan, E., Gui, Y., Yuan, L., Beyler, S.A., and Lessey, B.A. (2000). Blockade of the alpha(v)beta(3) integrin adversely affects implantation in the mouse. *Biol. Reprod.* 62, 1285–1290. <https://doi.org/10.1095/biolreprod62.5.1285>.
8. Haouzi, D., Dechaud, H., Assou, S., Monzo, C., de Vos, J., and Hamamah, S. (2011). Transcriptome analysis reveals dialogues between human trophoblast and endometrial cells during the implantation period. *Hum. Reprod.* 26, 1440–1449. <https://doi.org/10.1093/humrep/der075>.
9. Freis, A., Roesner, S., Marshall, A., Rehnitz, J., von Horn, K., Capp, E., Dietrich, J.E., Strowitzki, T., and Germeyer, A. (2021). Non-invasive embryo assessment: altered individual protein profile in spent culture media from embryos transferred at Day 5. *Reprod. Sci.* 28, 1866–1873. <https://doi.org/10.1007/s43032-020-00362-9>.
10. Licht, P., Russu, V., Lehmyer, S., and Wildt, L. (2001). Molecular aspects of direct LH/hCG effects on human endometrium—lessons from intrauterine microdialysis in the human female *in vivo*. *Reprod. Biol.* 1, 10–19.
11. Tu, Z., Wang, Q., Cui, T., Wang, J., Ran, H., Bao, H., Lu, J., Wang, B., Lydon, J.P., DeMayo, F., et al. (2016). Uterine RAC1 via Pak1-ERM signaling directs normal luminal epithelial integrity conducive to on-time embryo implantation in mice. *Cell Death Differ.* 23, 169–181. <https://doi.org/10.1038/cdd.2015.98>.
12. Wang, W., Vilella, F., Alarma, P., Moreno, I., Mignardi, M., Isakova, A., Pan, W., Simon, C., and Quake, S.R. (2020). Single-cell transcriptomic atlas of the human endometrium during the menstrual cycle. *Nat. Med.* 26, 1644–1653. <https://doi.org/10.1038/s41591-020-1040-z>.

(B) Bar plot showing the predicted cell ratio of human luminal epithelial cells based on three types of mouse luminal epithelial cells.

(C) Venn diagram showing embryo-derived signal conservation between mice and humans at the ligand-receptor level and pathway level.

(D) UMAP showing the cell types in the epithelium of thin and control endometrium (left). UMAP showing the distribution of the cells labeled based on the Scissor tools. The red and blue points are cells associated with thin and control endometrial phenotypes, respectively (middle). Bar plot showing the distribution of Scissor (+) and Scissor (-) cells of different cell types in the human endometrium (right).

(E) UMAP showing the cell types in the endometrium of RIF patients (left). UMAP showing the distribution of the cells labeled based on the Scissor tools. The red and blue points are cells associated with RIF and control endometrial phenotypes, respectively (middle). Bar plot showing the distribution of Scissor (+) and Scissor (-) cells in the endometrium of RIF patients (right).

(F) Bar plot showing ssGSEA scores of enriched GO terms among the DEGs between Scissor (+) and Scissor (-) cells in SOX9-positive cells from thin endometrium patients.

(G) Bar plot showing GSEA scores of enriched GO terms among the DEGs between Scissor (+) and Scissor (-) cells in luminal epithelial cells from RIF patients. See also [Figures S4–S6](#).

13. Stevens, A., Khashkhusha, T., Sharps, M., Garner, T., Ruane, P.T., and Aplin, J.D. (2023). The human early maternal–embryonic interactome. *Reprod. Med.* 4, 40–56. <https://doi.org/10.3390/reprodmed4010006>.
14. Svensson, V., Vento-Tormo, R., and Teichmann, S.A. (2018). Exponential scaling of single-cell RNA-seq in the past decade. *Nat. Protoc.* 13, 599–604. <https://doi.org/10.1038/nprot.2017.149>.
15. Blum, A., Mostow, K., Jackett, K., Kelty, E., Dakpa, T., Ryan, C., and Hagos, E. (2021). KLF4 regulates metabolic homeostasis in response to stress. *Cells* 10. <https://doi.org/10.3390/cells10040830>.
16. Nakamura, T., Yabuta, Y., Okamoto, I., Aramaki, S., Yokobayashi, S., Kurimoto, K., Sekiguchi, K., Nakagawa, M., Yamamoto, T., and Saitou, M. (2015). SC3-seq: a method for highly parallel and quantitative measurement of single-cell gene expression. *Nucleic Acids Res.* 43, e60. <https://doi.org/10.1093/nar/gkv134>.
17. Garcia-Alonso, L., Handfield, L.F., Roberts, K., Nikolakopoulou, K., Fernando, R.C., Gardner, L., Woodhams, B., Arutyunyan, A., Polanski, K., Hoo, R., et al. (2021). Mapping the temporal and spatial dynamics of the human endometrium in vivo and in vitro. *Nat. Genet.* 53, 1698–1711. <https://doi.org/10.1038/s41588-021-00972-2>.
18. Lv, H., Zhao, G., Jiang, P., Wang, H., Wang, Z., Yao, S., Zhou, Z., Wang, L., Liu, D., Deng, W., et al. (2022). Deciphering the endometrial niche of human thin endometrium at single-cell resolution. *Proc. Natl. Acad. Sci. USA* 119. <https://doi.org/10.1073/pnas.2115912119>.
19. Lédée, N., Munaut, C., Aubert, J., Sérazin, V., Rahmati, M., Chaouat, G., Sandra, O., and Foidart, J.M. (2011). Specific and extensive endometrial deregulation is present before conception in IVF/ICSI repeated implantation failures (IF) or recurrent miscarriages. *J. Pathol.* 225, 554–564. <https://doi.org/10.1002/path.2948>.
20. Pathare, A.D.S., Zaveri, K., and Hinduja, I. (2017). Downregulation of genes related to immune and inflammatory response in IVF implantation failure cases under controlled ovarian stimulation. *Am. J. Reprod. Immunol.* 78. <https://doi.org/10.1111/aji.12679>.
21. Hirota, Y. (2019). Progesterone governs endometrial proliferation-differentiation switching and blastocyst implantation. *Endocr. J.* 66, 199–206. <https://doi.org/10.1507/endocrj.EJ18-0431>.
22. Dey, S.K., Lim, H., Das, S.K., Reese, J., Paria, B.C., Daikoku, T., and Wang, H. (2004). Molecular cues to implantation. *Endocr. Rev.* 25, 341–373. <https://doi.org/10.1210/er.2003-0020>.
23. Haraguchi, H., Saito-Fujita, T., Hirota, Y., Egashira, M., Matsumoto, L., Matsuo, M., Hiraoka, T., Koga, K., Yamauchi, N., Fukayama, M., et al. (2014). MicroRNA-200a locally attenuates progesterone signaling in the cervix, preventing embryo implantation. *Mol. Endocrinol.* 28, 1108–1117. <https://doi.org/10.1210/me.2014-1097>.
24. Gebril, M., Hirota, Y., Aikawa, S., Fukui, Y., Kaku, T., Matsuo, M., Hirata, T., Akaeda, S., Hiraoka, T., Shimizu-Hirota, R., et al. (2020). Uterine epithelial progesterone receptor governs uterine receptivity through epithelial cell differentiation. *Endocrinology* 161. <https://doi.org/10.1210/endocr/bqaa195>.
25. Fukui, Y., Hirota, Y., Matsuo, M., Gebril, M., Akaeda, S., Hiraoka, T., and Osuga, Y. (2019). Uterine receptivity, embryo attachment, and embryo invasion: multistep processes in embryo implantation. *Reprod. Med. Biol.* 18, 234–240. <https://doi.org/10.1002/rmb2.12280>.
26. Lee, K., Jeong, J., Kwak, I., Yu, C.T., Lanske, B., Soegiarto, D.W., Toftgard, R., Tsai, M.J., Tsai, S., Lydon, J.P., et al. (2006). Indian hedgehog is a major mediator of progesterone signaling in the mouse uterus. *Nat. Genet.* 38, 1204–1209. <https://doi.org/10.1038/ng1874>.
27. Li, Q., Kannan, A., DeMayo, F.J., Lydon, J.P., Cooke, P.S., Yamagishi, H., Srivastava, D., Bagchi, M.K., and Bagchi, I.C. (2011). The antiproliferative action of progesterone in uterine epithelium is mediated by Hand2. *Science* 331, 912–916. <https://doi.org/10.1126/science.1197454>.
28. Xin, Q., Kong, S., Yan, J., Qiu, J., He, B., Zhou, C., Ni, Z., Bao, H., Huang, L., Lu, J., et al. (2018). Polycomb subunit BMI1 determines uterine progesterone responsiveness essential for normal embryo implantation. *J. Clin. Invest.* 128, 175–189. <https://doi.org/10.1172/JCI92862>.
29. Xie, H., Tranguch, S., Jia, X., Zhang, H., Das, S.K., Dey, S.K., Kuo, C.J., and Wang, H. (2008). Inactivation of nuclear Wnt-beta-catenin signaling limits blastocyst competency for implantation. *Development* 135, 717–727. <https://doi.org/10.1242/dev.015339>.
30. Frank, J.W., Seo, H., Burghardt, R.C., Bayless, K.J., and Johnson, G.A. (2017). ITGAV (alpha v integrins) bind SPP1 (osteopontin) to support trophoblast cell adhesion. *Reprod. Camb. Engl.* 153, 695–706. <https://doi.org/10.1530/REP-17-0043>.
31. Fujii, H., Tatsumi, K., Kosaka, K., Yoshioka, S., Fujiwara, H., and Fujii, S. (2006). Eph-ephrin A system regulates murine blastocyst attachment and spreading. *Dev. Dyn.* 235, 3250–3258. <https://doi.org/10.1002/dvdy.20977>.
32. Kim, H., Shin, J.E., Koo, H.S., Kwon, H., Choi, D.H., and Kim, J.H. (2019). Effect of autologous platelet-rich plasma treatment on refractory thin endometrium during the frozen embryo transfer cycle: a pilot study. *Front. Endocrinol. (Lausanne)* 10, 61. <https://doi.org/10.3389/fendo.2019.00061>.
33. Russell, S.J., Kwok, Y.S.S., Nguyen, T.T.N., and Librach, C. (2022). Autologous platelet-rich plasma improves the endometrial thickness and live birth rate in patients with recurrent implantation failure and thin endometrium. *J. Assist. Reprod. Genet.* 39, 1305–1312. <https://doi.org/10.1007/s10815-022-02505-0>.
34. Song, C., Yang, Z., Dong, D., Xu, J., Wang, J., Li, H., Huang, Y., Lan, X., Lei, C., Ma, Y., et al. (2019). miR-483 inhibits bovine myoblast cell proliferation and differentiation via IGF1/PI3K/AKT signal pathway. *J. Cell. Physiol.* 234, 9839–9848. <https://doi.org/10.1002/jcp.27672>.
35. Meng, Z., Feng, G., Hu, X., Yang, L., Yang, X., and Jin, Q. (2021). SDF Factor-1alpha promotes the migration, proliferation, and osteogenic differentiation of mouse bone marrow mesenchymal stem cells through the Wnt/beta-catenin pathway. *Stem Cells Dev.* 30, 106–117. <https://doi.org/10.1089/scd.2020.0165>.
36. RoyChoudhury, S., Singh, A., Gupta, N.J., Srivastava, S., Joshi, M.V., Chakravarty, B., and Chaudhury, K. (2016). Repeated implantation failure versus repeated implantation success: discrimination at a metabolomic level. *Hum. Reprod.* 31, 1265–1274. <https://doi.org/10.1093/humrep/dew064>.
37. Cho, S.H., Kim, J.H., An, H.J., Kim, J.O., Kim, Y.R., Lee, W.S., and Kim, N.K. (2021). Association of methionine synthase (rs1805087), methionine synthase reductase (rs1801394), and methylenetetrahydrofolate dehydrogenase 1 (rs2236225) genetic polymorphisms with recurrent implantation failure. *Hum. Fertil. (Camb)* 24, 161–168. <https://doi.org/10.1080/14647273.2019.1613679>.
38. Lai, Z.Z., Wang, Y., Zhou, W.J., Liang, Z., Shi, J.W., Yang, H.L., Xie, F., Chen, W.D., Zhu, R., Zhang, C., et al. (2022). Single-cell transcriptome profiling of the human endometrium of patients with recurrent implantation failure. *Theranostics* 12, 6527–6547. <https://doi.org/10.7150/thno.74053>.
39. Rubel, C.A., Lanz, R.B., Kommagani, R., Franco, H.L., Lydon, J.P., and DeMayo, F.J. (2012). Research resource: genome-wide profiling of progesterone receptor binding in the mouse uterus. *Mol. Endocrinol.* 26, 1428–1442. <https://doi.org/10.1210/me.2011-1355>.
40. Zhou, F., Wang, R., Yuan, P., Ren, Y., Mao, Y., Li, R., Lian, Y., Li, J., Wen, L., Yan, L., et al. (2019). Reconstituting the transcriptome and DNA methylation landscapes of human implantation. *Nature* 572, 660–664. <https://doi.org/10.1038/s41586-019-1500-0>.
41. Kim, D., Langmead, B., and Salzberg, S.L. (2015). HISAT: a fast spliced aligner with low memory requirements. *Nat. Methods* 12, 357–360. <https://doi.org/10.1038/nmeth.3317>.
42. Liao, Y., Smyth, G.K., and Shi, W. (2014). featureCounts: an efficient general purpose program for assigning sequence reads to genomic features. *Bioinformatics* 30, 923–930. <https://doi.org/10.1093/bioinformatics/btt656>.
43. Ritchie, M.E., Phipson, B., Wu, D., Hu, Y., Law, C.W., Shi, W., and Smyth, G.K. (2015). limma powers differential expression analyses for RNA-sequencing and microarray studies. *Nucleic Acids Res.* 43, e47. <https://doi.org/10.1093/nar/gkv007>.

Developmental Cell Resource



44. Zheng, G.X., Terry, J.M., Belgrader, P., Ryvkin, P., Bent, Z.W., Wilson, R., Ziraldo, S.B., Wheeler, T.D., McDermott, G.P., Zhu, J., et al. (2017). Massively parallel digital transcriptional profiling of single cells. *Nat. Commun.* 8, 14049. <https://doi.org/10.1038/ncomms14049>.
45. Dobin, A., Davis, C.A., Schlesinger, F., Drenkow, J., Zaleski, C., Jha, S., Batut, P., Chaisson, M., and Gingeras, T.R. (2013). STAR: ultrafast universal RNA-seq aligner. *Bioinformatics* 29, 15–21. <https://doi.org/10.1093/bioinformatics/bts635>.
46. Hao, Y., Hao, S., Andersen-Nissen, E., Mauck, W.M., 3rd, Zheng, S., Butler, A., Lee, M.J., Wilk, A.J., Darby, C., Zager, M., et al. (2021). Integrated analysis of multimodal single-cell data. *Cell* 184, 3573–3587.e29. <https://doi.org/10.1016/j.cell.2021.04.048>.
47. Trapnell, C., Cacchiarelli, D., Grimsby, J., Pokharel, P., Li, S., Morse, M., Lennon, N.J., Livak, K.J., Mikkelsen, T.S., and Rinn, J.L. (2014). The dynamics and regulators of cell fate decisions are revealed by pseudotemporal ordering of single cells. *Nat. Biotechnol.* 32, 381–386. <https://doi.org/10.1038/nbt.2859>.
48. Aibar, S., González-Blas, C.B., Moerman, T., Huynh-Thu, V.A., Imrichova, H., Hulselmans, G., Rambow, F., Marine, J.C., Geurts, P., Aerts, J., et al. (2017). SCENIC: single-cell regulatory network inference and clustering. *Nat. Methods* 14, 1083–1086. <https://doi.org/10.1038/nmeth.4463>.
49. Jin, S., Guerrero-Juarez, C.F., Zhang, L., Chang, I., Ramos, R., Kuan, C.H., Myung, P., Plikus, M.V., and Nie, Q. (2021). Inference and analysis of cell-cell communication using CellChat. *Nat. Commun.* 12, 1088. <https://doi.org/10.1038/s41467-021-21246-9>.
50. Wu, T., Hu, E., Xu, S., Chen, M., Guo, P., Dai, Z., Feng, T., Zhou, L., Tang, W., Zhan, L., et al. (2021). clusterProfiler 4.0: a universal enrichment tool for interpreting omics data. *Innovation (Camb)* 2, 100141. <https://doi.org/10.1016/j.xinn.2021.100141>.
51. Hänelmann, S., Castelo, R., and Guinney, J. (2013). GSVA: gene set variation analysis for microarray and RNA-seq data. *BMC Bioinformatics* 14, 7. <https://doi.org/10.1186/1471-2105-14-7>.
52. Korsunsky, I., Millard, N., Fan, J., Slowikowski, K., Zhang, F., Wei, K., Baglaenko, Y., Brenner, M., Loh, P.R., and Raychaudhuri, S. (2019). Fast, sensitive and accurate integration of single-cell data with Harmony. *Nat. Methods* 16, 1289–1296. <https://doi.org/10.1038/s41592-019-0619-0>.
53. Shannon, P., Markiel, A., Ozier, O., Baliga, N.S., Wang, J.T., Ramage, D., Amin, N., Schwikowski, B., and Ideker, T. (2003). Cytoscape: a software environment for integrated models of biomolecular interaction networks. *Genome Res.* 13, 2498–2504. <https://doi.org/10.1101/gr.123930>.
54. Harris, M.A., Clark, J., Ireland, A., Lomax, J., Ashburner, M., Foulger, R., Eilbeck, K., Lewis, S., Marshall, B., Mungall, C., et al. (2004). The gene ontology (GO) database and informatics resource. *Nucleic Acids Res.* 32, D258–D261. <https://doi.org/10.1093/nar/gkh036>.
55. Kanehisa, M., and Goto, S. (2000). KEGG: Kyoto Encyclopedia of Genes and Genomes. *Nucleic Acids Res.* 28, 27–30. <https://doi.org/10.1093/nar/28.1.27>.

STAR★METHODS

KEY RESOURCES TABLE

REAGENT or RESOURCE	SOURCE	IDENTIFIER
Antibodies		
TACSTD2	Abcam	Cat# ab271996; RRID: NA
MKI67	Abcam	Cat# ab16667; RRID: AB_302459
β-catenin	Abcam	Cat# ab32572; RRID: AB_725966
DIG-AP	Roche	Cat# 11093274910; RRID: AB_514497
Goat Anti-Rabbit IgG H&L (Alexa Fluor® 594)	Abcam	Cat# ab150080; RRID: AB_2650602
Goat Anti-Rabbit IgG H&L (HRP)	ZSGB-BIO	Cat# PV-6001; RRID: AB_2864333
Biological samples		
Human endometrial samples	the Reproductive Medicine Center of the Affiliated Drum Tower Hospital of Nanjing University Medical School	N/A
Chemicals, peptides, and recombinant proteins		
recombinant murine EGF	Peprotech	Cat# 315-09
recombinant human FGF-10	Peprotech	Cat# 100-26
recombinant human Noggin	Peprotech	Cat# 120-10C
recombinant human R-spondin-1	Peprotech	Cat# 120-38
recombinant murine Wnt-3a	Peprotech	Cat# 315-20
E2	Sigma	Cat# E2758
P4	XIANJU PHAMA	Cat# H33020828
sesame oil	Sigma	Cat# S3547
A83-01	MCE	Cat# HY-10432
N2 supplement	Gibco	Cat# 17502-048
B27 supplement	Gibco	Cat# 17504-044
Nicotinamide	Sigma	Cat# N3376
GlutaMax	Gibco	Cat# 35050061
insulin-transferrin-selenium	Gibco	Cat# 41400-045
Matrigel	CORNING	Cat# 356231
Dispase	Sigma	Cat# D4693
Trypsin	Sigma	Cat# T4799
Imatinib	MCE	Cat# HY-15463
Critical commercial assays		
All-In-One 5X RT MasterMix	ABM	Cat# G592
BCIP/NBT Alkaline Phosphatase Color Development Kit	Beyotime	Cat# C3206
DAB Substrate kit	ZSGB-BIO	Cat# ZLI-9018
Deposited data		
scRNAseq data of mouse endometrium(2.5-4.5DPC)	In this study	GSA:CRA011266
scRNAseq data of mouse endometrium(2.5-4.5DPP)	In this study	GSA:CRA011267
Bulk RNAseq data of mouse embryos (E3.5 and E4.0)	In this study	GSA:CRA011264
Bulk RNAseq data from patients with thin endometrium	In this study	GSA:HRA004631
scRNAseq data from patients with RIF	In this study	GSA:HRA004756
ChIP-seq data of mouse uterus	Rubel et al. ³⁹	GEO:GSE34927
scRNAseq data of mouse embryo(E4.5)	Nakamura et al. ¹⁶	GEO:GSE63266
scRNAseq data of human endometrium	Wang et al. ¹²	GEO:GSE111976
scRNAseq data of human embryos	Zhou et al. ⁴⁰	GEO:GSE109555

(Continued on next page)

Developmental Cell Resource



Continued

REAGENT or RESOURCE	SOURCE	IDENTIFIER
scRNASeq data from patients with thin endometrium	Lv et al. ¹⁸	SRA: PRJNA730360
Microarray data from patients with RIF	Lédee et al. ¹⁹	GEO:GSE26787
Microarray data from patients with RIF	Pathare et al. ²⁰	GEO:GSE92324
Experimental models: Organisms/strains		
Mouse: ICR	Nanjing Medical University	N/A
Oligonucleotides		
siRNA target sequences against mEpha1 #1: GGATGCAAAGAGACCTTCA	This paper	N/A
siRNA target sequences against mEpha1 #2: CACCACATCTACCGTGCAA	This paper	N/A
siRNA target sequences against mEpha1 #3: CCACATACATTCTCAGAGT	This paper	N/A
Primers for real-time qPCR and ISH probes, See Table S2	This paper	N/A
Software and algorithms		
HISAT2	Kim et al. ⁴¹	v2.2.1
FeatureCounts	Liao et al. ⁴²	v2.0.1
limma	Ritchie et al. ⁴³	v3.52.1
ggplot2	https://cran.r-project.org/	v3.3.6
R software	https://www.R-project.org/	v4.1.3
Cell Ranger	Zheng et al. ⁴⁴	v1.2.1
STAR	Dobin et al. ⁴⁵	v2.5.4a
Seurat	Hao et al. ⁴⁶	v4.1.1
Monocle2	Trapnell et al. ⁴⁷	v2.22.0
SCENIC	Aibar et al. ⁴⁸	v1.2.4
cisTarget databases	https://www.bioconductor.org/	v1.14.0
AUCell	https://www.bioconductor.org/	v1.16.0
Cytoscape software	https://cytoscape.org/	v3.5.1
CellChat	Jin et al. ⁴⁹	v1.1.3
ClusterProfiler	Wu et al. ⁵⁰	v4.2.2
GSVA package	Hänzelmann et al. ⁵¹	v1.42.0
GraphPad Prism	https://www.graphpad.com/	version 9.0

RESOURCE AVAILABILITY

Lead contact

Further information and requests for reagents should be directed to and will be fulfilled by the Lead Contact, Haixiang Sun (stevensunz@163.com)

Materials availability

This study did not generate new unique reagents. All stable reagents in this study are available from the [lead contact](#) with a completed material transfer agreement.

Data and code availability

- Single-cell RNA-seq data have been deposited at Genome Sequence Archive (GSA) and Genome Sequence Archive for Human. Accession numbers are listed in the [key resources table](#).
- This paper does not report original code.
- Any additional information required to access and analyze the data reported in this paper is available from the [lead contact](#) upon request.

EXPERIMENTAL MODEL AND STUDY PARTICIPANT DETAILS

Patients and samples

Informed consent was acquired from all patients prior to undergoing the routine biopsy procedure to determine the status of the endometrium and the use of samples (including endometrial tissues at the late proliferative stage from thin endometrium and fertile women and endometrial tissues at the mid-secretion stage from RIF and fertile women) was approved by the ethics committee of the Affiliated Drum Tower Hospital of Nanjing University Medical School on 5 December 2013 (2013-081-01). This research was carried out in the Reproductive Medicine Center of the Affiliated Drum Tower Hospital of Nanjing University Medical School.

In total, 12 thin endometrium patients and 9 corresponding contemporaneous fertile patients were recruited to obtain uterine tissue for bulk RNA-seq (6 vs. 3), scRNA-seq (3 vs. 3) and subsequent experimental verification (3 vs. 3). The criteria for the diagnosis of thin endometrium were age < 40 years old and endometrial thickness < 8 mm in 2 previous endometrial preparation ART cycles. The normal controls had normal menstrual volume and normal ovarian function, and the endometrial thickness was ≥ 8 mm. Patients with moderate and severe intrauterine adhesions, intrauterine developmental malformations, endometriosis and adenomyosis, previous tuberculosis infection, submucosal fibroids, endometrial polyps, and hormone replacement contraindications were excluded.

In addition, 3 RIF patients were enrolled to obtain uterine tissue for scRNA-seq (Table S3). The diagnosis of RIF should meet the following criteria: 1) < 40 years old, ≥ 3 embryo transfer cycles failed, or 2) < 40 years old, ≥ 2 embryo transfer cycles failed and ≥ 4 high-quality cleavage embryos or ≥ 2 high-quality blastocysts or ≥ 2 high-quality cleavage embryos and 1 high-quality blastocyst transferred. During the sampling period, no glucocorticoids, antibiotics, or vaginal drugs were used, no cervical therapy was performed within 1 week, no vaginal flushing was performed within 5 days, and no sexual activity was performed within 1 month. Women with intrauterine adhesion, mechanical injury to the endometrium, uterine malformations, untreated hydrosalpinx, submucosal or intramural uterine fibroids > 4 cm, adenomyosis, stage III-IV endometriosis, endometritis with a definite pathological diagnosis, and chromosomal abnormalities were excluded.

Mice

Eight-week-old ICR female and male mice were purchased from Nanjing Medical University (Nanjing, China) and were maintained in the Animal Laboratory Center of Nanjing Drum Tower Hospital (Nanjing, China) with a 12/12 h light/dark cycle (lights off at 1900 hours) and food and water available ad libitum. All mouse experiments in this study were approved by the Institutional Animal Care and Use Committee of Nanjing Drum Tower Hospital (SYXK 2019-0059).

METHOD DETAILS

Uterine tissue collection

Eight-week-old ICR female mice were mated with fertile males. The morning that a vaginal plug was observed was termed day 0.5 of the pregnancy. For sequencing, we prepared two female mice for each designated time point (2.5, 3.5, 4.0 and 4.5 DPC) as pregnant group. We collected one half of the bicornuate uterus from each pregnant mouse, pooled them, and performed scRNaseq. The contralateral side of the uterus was collected and subjected to embryo flushing for bulk RNaseq. To distinguish maternal and embryonic signaling, we also collected the uteri of pseudopregnant mice at corresponding time points (2.5, 3.5, 4.0 and 4.5 DPP) for scRNaseq.

Ovariectomy and hormone induction models

Eight-week-old ICR female mice were rested for 2 weeks after ovariectomy. Then, 50 µL of sesame oil containing 100 ng E2 was injected subcutaneously for 3 consecutive days. The mice were allowed to rest for another 2 days, and then 50 µL of sesame oil containing 1 mg P4 and 10 ng E2 was injected subcutaneously for 2 consecutive days. The uterine tissues from the mice at 2 weeks after ovariectomy, 6 h after receiving only the E2 injection, 2 days after receiving only the E2 injection, and 6 h after receiving the P4+E2 injection were collected.

Bulk RNA-seq library preparation and data analysis

Total RNA was isolated and used for RNA-seq analyses, and a cDNA library was constructed by Beijing Genomics Institute using an Illumina HiSeq X platform (Shenzhen, China). High-quality reads were aligned to the mouse reference genome (mm10) using HISAT2 (v2.2.1).⁴¹ The expression levels of each gene were calculated using FeatureCounts (v2.0.1) software.⁴² A differentially expressed gene (DEG) analysis was performed using the limma package (v3.52.1),⁴³ and all graphics were drawn with the ggplot package (v3.3.6) in R software (v4.1.3).

10X Genomics library preparation, sequencing, and acquisition of an expression matrix

An scRNA-seq library was constructed following the 10X Genomics scRNA-seq protocol. Briefly, suspensions containing ~10K cells were diluted following the instrument manufacturer's recommendations and mixed with buffer before being loaded into a 10× Chromium Controller using Chromium Single Cell 3' v3 reagents. Each sequencing library was prepared following the manufacturer's instructions. The resulting libraries were then sequenced on an Illumina NovaSeq 6000 (Illumina, San Diego).

Raw sequencing data were demultiplexed using the mkfastq application (Cell Ranger v1.2.1⁴⁴). Three types of fastq files were generated: I1 contained an 8-bp sample index; R1 contained a 26-bp (10-bp cell [BC] + 16-bp unique molecular identifier [UMI]) index; and R2 contained a 100-bp cDNA sequence. The Fastq files were then run with the cellranger count application (Cell Ranger v1.2.1⁴⁴) using default settings to perform alignment (using STAR v2.5.4a⁴⁵), filtering, cell barcode counting, and UMI counting. The UMI count tables for each cell barcode were used for further analysis.

Data processing, batch effect correction and cell identification

We used the Seurat package(v4.1.1)⁴⁶ to perform further analyses. Specifically, the UMI-based count matrix was first read into R using the Read10X function, and cells in which the number of genes was fewer than 500 or in which the mitochondrial gene ratio was more than 15% were considered low-quality cells and were removed. Finally, the remaining cells were used for subsequent analyses.

The NormalizeData function with default parameters was used to normalize the data. Then, the mean-variable of each gene was calculated using the vst algorithm in the FindVariableFeatures function, and 2,000 genes that induced the greatest differences among cells, that is, highly variable genes (HVGs), were selected. The ScaleData function was used to standardize the data for subsequent dimension reduction analysis.

We used the selected HVGs in a principal component analysis (PCA), then selected the top 10 principal components for batch correction with the harmony algorithm⁵² and used uniform manifold approximation and projection (UMAP) for further dimension reduction. For the identification of all cells, we first applied the FindNeighbor function to build a network and then used the FindCluster function to perform unsupervised cell clustering. The FindMarkers function was then used, and genes with log₂-fold change (FC) >1 and p.adj <0.001 criteria were markers and used to annotate cell populations.

Pseudotime analysis

We used the Monocle2 package(v2.22.0)⁴⁷ to construct a cell differentiation trajectory. Specifically, the UMI-based count matrix was read into R, and a CellDataSet was constructed (in Monocle). The HVGs selected by Seurat were used as the genes to calculate pseudotime, and the DDRTree algorithm in the reduceDimension function was used to construct a cell differentiation trajectory.

Correlation analysis

For correlation analysis, we calculated the average expression levels of the transcriptome for each cell type using the “AverageExpression()” function in Seurat package and then calculated the Pearson correlation coefficient between all cell populations obtained from both the pregnancy and pseudopregnancy groups.

Transcription factor-related gene regulation subnetwork analysis

Regulatory network and regulon activity analyses were performed on a mouse (mm10) dataset (10 kb around TSS feature database downloaded from <https://resources.aertslab.org/>) using the SCENIC package (v1.2.4).⁴⁸ The UMI-based count matrix was used as input to identify coexpression modules through the GRNBoost2 algorithm. Then, regulons were derived by identifying the direct-binding transcription factor (TF) targets while pruning other regulons based on motif enrichment around transcription start sites (TSSs) in cisTarget databases(v1.14.0). Using AUCCell(v1.16.0), the regulon activity score was determined as the area under the recovery curve (AUC), and the regulon status as active/inactive was identified based on the predicted AUC default threshold for each regulon in all cells. Subsequently, using a binarize function, we obtained the binary regulon activity score, which was converted into “ON/OFF” (i.e., 1/0) labels. Furthermore, we removed regulons that were not active in at least 1% of the cells. We used a cutoff of 1% because it closely approximates the smallest cluster of the cells in our analysis, allowing the identification of regulons that were active in rare cell groups.

Some TFs that targeted genes were regulated by other TFs in some regulons. Therefore, based on the relationships between these TFs, we constructed a network to identify the core TFs using Cytoscape software (v3.5.1).⁵³

Cell-cell communication analysis

To identify and visualize cell-cell interactions, we employed an R package named CellChat (v1.1.3).⁴⁹ In brief, we followed the official workflow, loaded the normalized counts into CellChat and applied the standard preprocessing steps, including those using the functions identifyOverExpressedGenes, identifyOverExpressedInteractions, and projectData with a standard parameter set. A total of 2,021 precompiled mouse ligand-receptor interactions were selectively used as a priori network information. We then calculated the potential ligand-receptor interactions between embryo and epithelial cells based on the functions computeCommunProb, computeCommunProbPathway, and aggregateNet using standard parameters.

Gene enrichment analysis

We performed Gene Ontology (GO)⁵⁴ and Kyoto Encyclopedia of Genes and Genomes (KEGG)⁵⁵ enrichment analyses using the enrichGO and enrichKEGG functions in the ClusterProfiler package (v4.2.2).⁵⁰ DEG lists were used as input, and the appropriate organism of interest was used as the background. Terms with corrected P values < 0.05 were considered significant.

We performed gene set enrichment analysis (GSEA) using gseGO and gseKEGG in the ClusterProfiler package. In summary, we sorted the log2FC values of the two groups and regarded them as the input for the gseGO/gseKEGG analyses. Terms with a

P value < 0.05 were considered significant. Finally, we performed a gene set variation analysis (GSVA) using the gsva function in the GSVA package (v1.42.0).⁵¹

ssGSEA

To conduct ssGSEA, we first identified differentially expressed genes between AECs, EECs, and SECs as the signatures for these cell types and then converted these genes to their homologs in humans. Next, we isolated human luminal epithelium data, including ciliated and nonciliated epithelium as well as SOX9-positive epithelium, from a published single-cell RNAseq dataset of the human endometrium. We reclustered these cells, which yielded 3 subtypes of ciliated epithelium, 8 subtypes of nonciliated epithelium, and 7 subtypes of SOX9-positive epithelium. We calculated the average expression of these signatures in these subpopulations of epithelial cells in humans, followed by calculating the ssGSEA scores using GSVA function in GSVA package. We used a threshold of 0.5, such that only cells with scores higher than 0.5 were considered similar to this cell type.

Real-time qPCR (RT-qPCR) verification

Total RNA was extracted from cells or tissues after treatment with TRIzol (Ambion) according to the manufacturer's instructions. The concentration and purity of all RNA were tested after extraction. Reverse transcription was performed to generate cDNA using 5× All-In-One RT MasterMix (Abm) for RT-qPCR, which was performed according to the instructions of ChamQ SYBR RT-qPCR Master Mix (Vazyme) and a qTOWER³G touch instrument (Analytik Jena). Data were analyzed using the $2^{-\Delta\Delta Ct}$ relative quantitative method in Microsoft Excel software. The primers used are listed in [Table S2](#). 18S rRNA served as an internal control.

In situ hybridization

In brief, frozen sections of mouse uterine were fixed in 4% paraformaldehyde at room temperature for 20 min. After acetylation buffer treatment, the sections were incubated with preheated denatured digoxin-labeled probe overnight at 60°C. On the second day, the sections were washed successively with hybrid wash solution, MABT solution and RNA wash solution. Then, 80 µl of 10 mg/ml RNase was added to the RNA wash solution, and the sections were incubated at 37°C for another 30 min. Next, the sections were washed successively with fresh RNA wash solution and MABT solution. After blocking, the sections were incubated with anti-digoxin antibodies (1:200, Roche) overnight at 4°C. On the third day, after washing with MABT solution and NTM solution, the sections were treated with 0.5 mg/mL levamisole for 10 min. Developing of the sections was according to the manufacturer's instructions of the BCIP/NBT (Beyotime Biotechnology) kit. Subsequently, the sections were stained with 0.1% nuclear fast red solution (Phygene) and mounted. The primers used to amplify probes are listed in [Table S2](#).

Immunohistochemistry staining

Tissue sections were immunostained overnight with primary antibodies against TACSTD2 (1:1000 dilution, Abcam) and MKI67 (1:1000 dilution, Abcam) at 4°C. Control sections were treated concurrently with nonspecific rabbit IgG. On the following day, the sections were incubated with a goat anti-rabbit secondary antibody at 37°C for 30 min. Next, the sections were stained with 3,3'-diaminobenzidine (DAB) and counterstained with hematoxylin.

Hematoxylin and eosin (H&E) staining

Implantation site tissues were fixed, and paraffin sections were subjected to hematoxylin and eosin staining. Briefly, paraffin sections were dewaxed, followed by staining the nuclei and cytoplasm with hematoxylin and eosin, respectively. Finally, the sections were dehydrated and mounted.

Immunofluorescence

Frozen sections of thin endometrium and control endometrium were mounted onto poly-L-lysine-coated slides and fixed in 4% paraformaldehyde. After washing with PBS, permeation was carried out with 0.5% Triton X-100. Then, sections were blocked in 3% BSA and incubated with primary antibody (β -catenin, 1:1000 dilution, Abcam) at 4°C overnight, followed by incubation in secondary antibody (Alexa 488-conjugated secondary antibody, Thermo) at room temperature for 1 h. Nuclear staining was performed using DAPI for 5 min. Immunofluorescence was visualized using a fluorescence microscope (LEICA DM3000 LED).

Mouse embryo transplantation assay

The mice at 3.5 DPC were sacrificed by neck dislocation, and blastocysts were recovered in M2 for future use. After anesthesia, 10 µl PDGFR inhibitor, imatinib (100 µM, MCE), or 30 µl EphA1 short interfering RNA (siRNA) mixture (20 µM) was injected into one uterine horn of the mice at 2.5 DPP, and the same amount of control fluid was injected into the other horn. Then blastocysts were transplanted into each side of the uterus. The specific siRNA sequences against EphA1 were GGATGCAAAGAGACCTTCA (#1), CACCACATCTACCGTGCAA (#2) and CCACATACATTCTCAGAGT (#3). 2 days later, the mouse uteruses were collected after Chicago blue dye injection.

Organoid culture from mouse endometrium

Whole mouse uterus was obtained at 2.5 DPC, cut to a length of approximately 1 cm, incubated in digestive enzyme solution (6 mg/ml Dispase + 25 mg/ml Trypsin). Since the luminal epithelium came into contact with the digestive enzyme solution first, we isolated

most of the luminal epithelium and little of the glandular epithelium by adjusting the first step digestion duration to 30 min at 37°C. Then, the luminal epithelial cells were extruded using a syringe needle and redigested into single cells at 37°C for another 30 min. The single luminal epithelial cells were resuspended in 75% Matrigel/25% DMEM/F12, plated as drops and cultured in DMEM/F12 containing a cocktail of growth and signaling factors (1% penicillin/streptomycin, 1% insulin-transferrin-selenium (ITS), 1×GlutaMax, 1 mM nicotinamide, 2% B27 supplement, 1% N2 supplement, 50 ng/ml recombinant mouse EGF, 100 ng/ml recombinant human FGF-10, 100 ng/ml recombinant human Noggin, 200 ng/ml Wnt3a, 200 ng/ml recombinant human R-spondin-1, 0.5 μM ALK5/7/4 inhibitor A83-01 and 2 nM β-estradiol). To be closer to physiological conditions, the whole process of organoids culture was maintained in an environment with a low concentration of estrogen (2 nM). Outgrowing organoids were passaged every 7–10 days after digestion.

Induction differentiation of endometrial organoids

After organoids formed in a basal medium containing low doses of estrogen, organoids were cultured with new medium containing 10 nM estrogen for 48 h, and then replaced the medium with: (1) organoid expansion medium + 10 nM estrogen; (2) organoid expansion medium + 10 nM estrogen + 1 μM progesterone, respectively. 48 h later, the organoids were collected for detection.

QUANTIFICATION AND STATISTICAL ANALYSIS

The data are expressed as the means ± SD. All experiments were performed at least three times. GraphPad Prism software (version 9.0) was used to perform statistical analyses. Statistical analyses were performed with one-way ANOVA for experiments involving more than two groups. P values < 0.05 were considered statistically significant.

Supplemental information

**Maternal and embryonic signals cause functional
differentiation of luminal epithelial cells
and receptivity establishment**

Hai-Quan Wang, Yang Liu, Dong Li, Jing-Yu Liu, Yue Jiang, Yuanlin He, Ji-Dong Zhou, Zhi-Long Wang, Xin-Yi Tang, Yang Zhang, Xin Zhen, Zhi-Wen Cao, Xiao-Qiang Sheng, Chao-Fan Yang, Qiu-Ling Yue, Li-Jun Ding, Ya-Li Hu, Zhi-Bin Hu, Chao-Jun Li, Gui-Jun Yan, and Hai-Xiang Sun

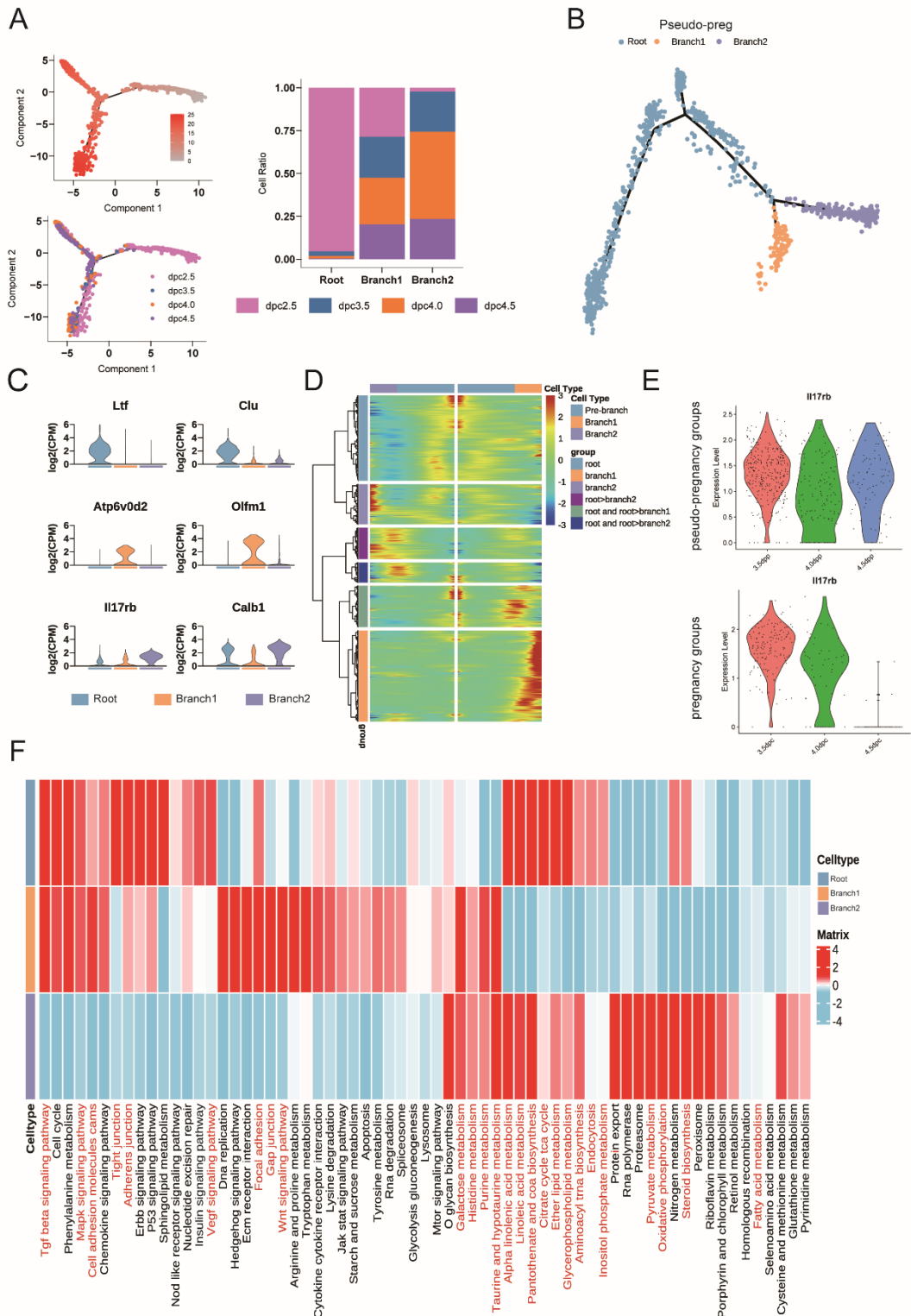


Figure S1: Pseudotime analysis of endometrial luminal epithelial cells in pregnant and pseudopregnant mice. Related to Fig. 3

(A) Dot plot showing cell trajectories ordered in pseudotime and at different time points, and bar plot showing the distribution of the three cell types at each time point. (B) Developmental pseudotime of

endometrial luminal epithelial cells in pseudopregnant mice. (C) Violin plot showing log2-transformed expression of marker genes in three types of luminal epithelial cells in mice. (D) Heatmap showing the hierarchical relationship between clusters of genes that were differentially expressed across pseudotimes of endometrial luminal epithelial cells in pregnant mice. (E) Violin plot showing log2-transformed expression of Il17rb in the pregnancy and pseudopregnancy groups. (F) Heatmap showing GSVA scores of KEGG pathways in all three types of luminal epithelial cells in mice.

A

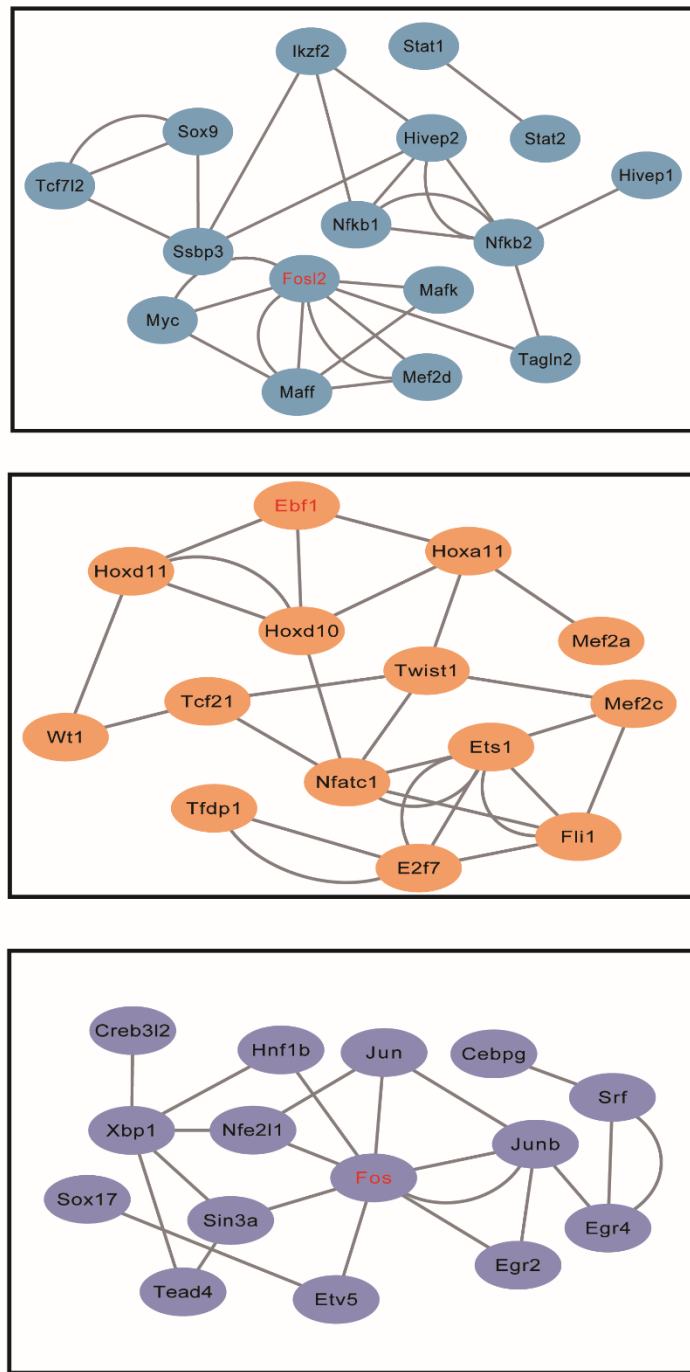


Figure S2: Regulatory networks of transcription factors during luminal epithelial cell differentiation. Related to Fig. 4

(A) Regulatory networks of transcription factors during luminal epithelial cell differentiation in roots (top), AECs (middle) and SECs (bottom).

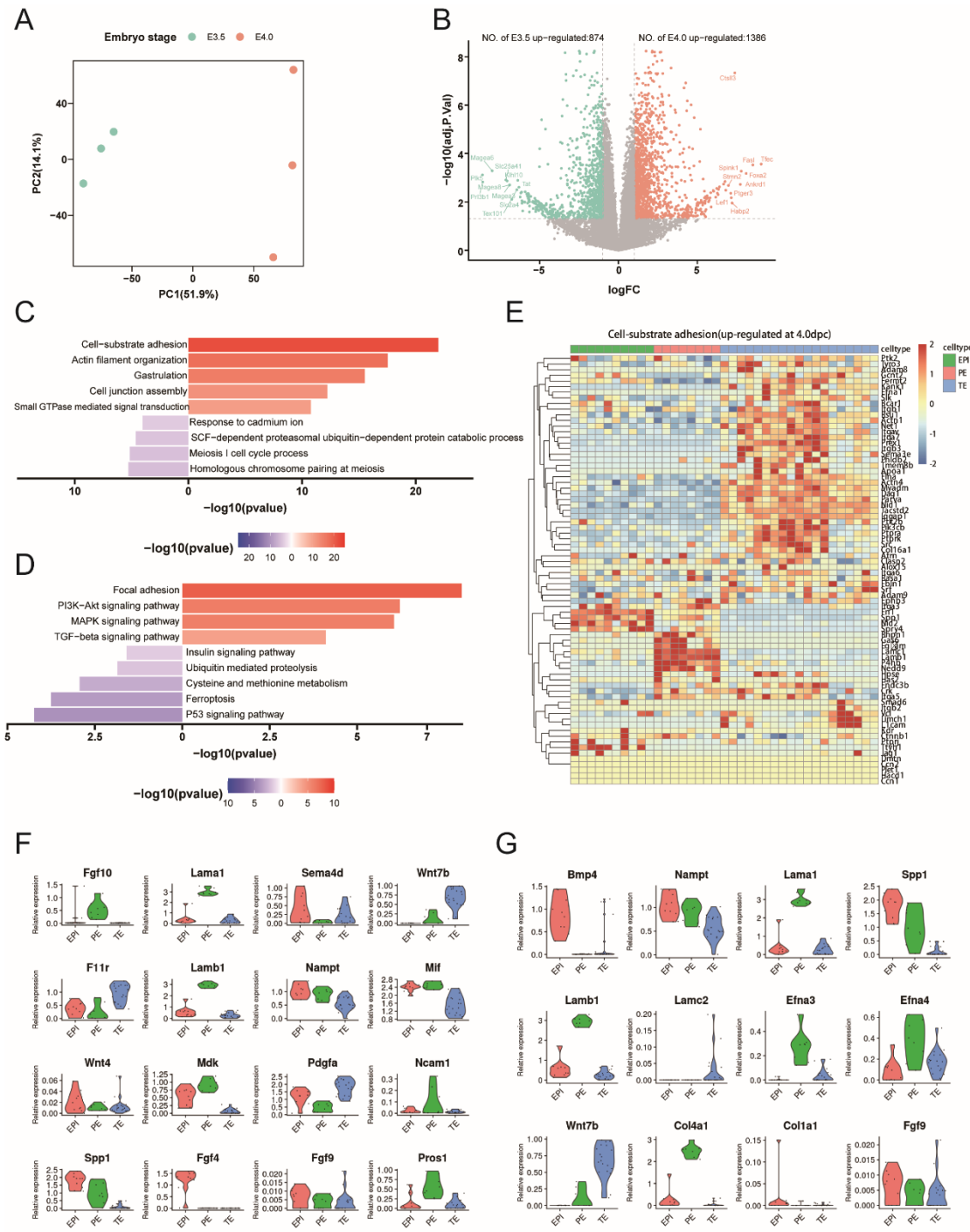


Figure S3: Transcriptome of mouse embryos at E3.5 and E4.0. Related to Fig. 5

(A) PCA plot showing the difference in the transcriptome of E3.5 and E4.0 mouse embryos. (B) Volcano plot showing DEGs between E3.5 and E4.0 mouse embryos. (C) Bar plot showing enriched GO biological process terms of DEGs between E3.5 and E4.0 mouse embryos. (D) Bar plot showing enriched KEGG pathways of DEGs between E3.5 and E4.0 mouse embryos. (E) Heatmap showing the expression of genes related to cell substrate adhesion in EPI/PE/TE (F) Violin plot showing ligands identified in Fig5C expressed in blastocyst. (G) Violin plot showing ligands identified in Fig6C expressed in

blastocyst.

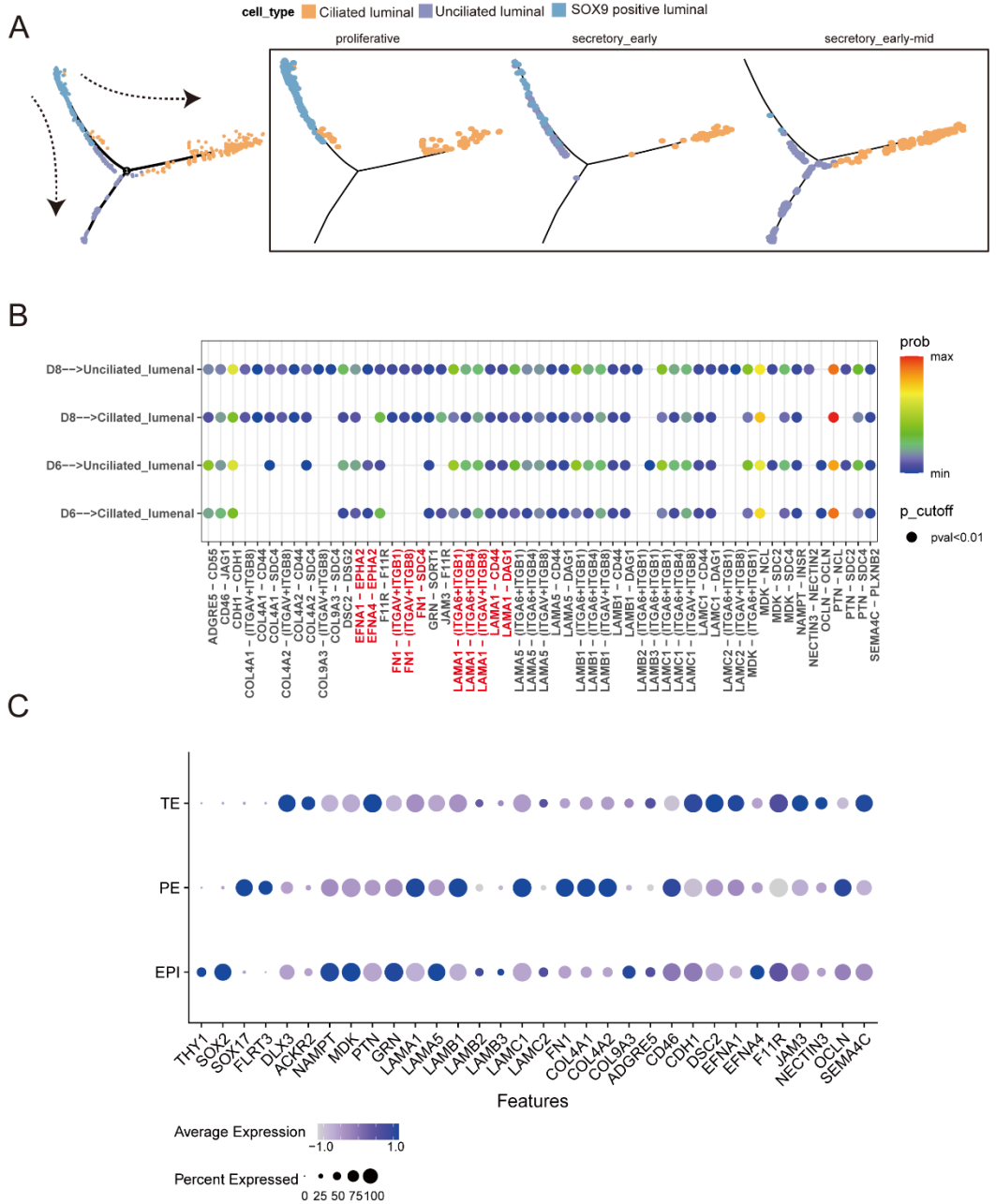


Figure S4: Both luminal epithelial cell differentiation and directed signaling are conserved in humans and mice. Related to Fig. 7

(A) Developmental pseudotime of endometrial luminal epithelial cells in the human uterus. (B) Dot plot showing embryo-derived signals from D6 and D8 communicating with ciliated luminal cells and unciliated luminal cells. Point size represents the P value, and the color represents the possibility of communication of the ligand–receptor pairs between embryo and luminal epithelial cells. (C) Dot plot showing the ligands identified in SFig. 4B expressed in blastocysts.

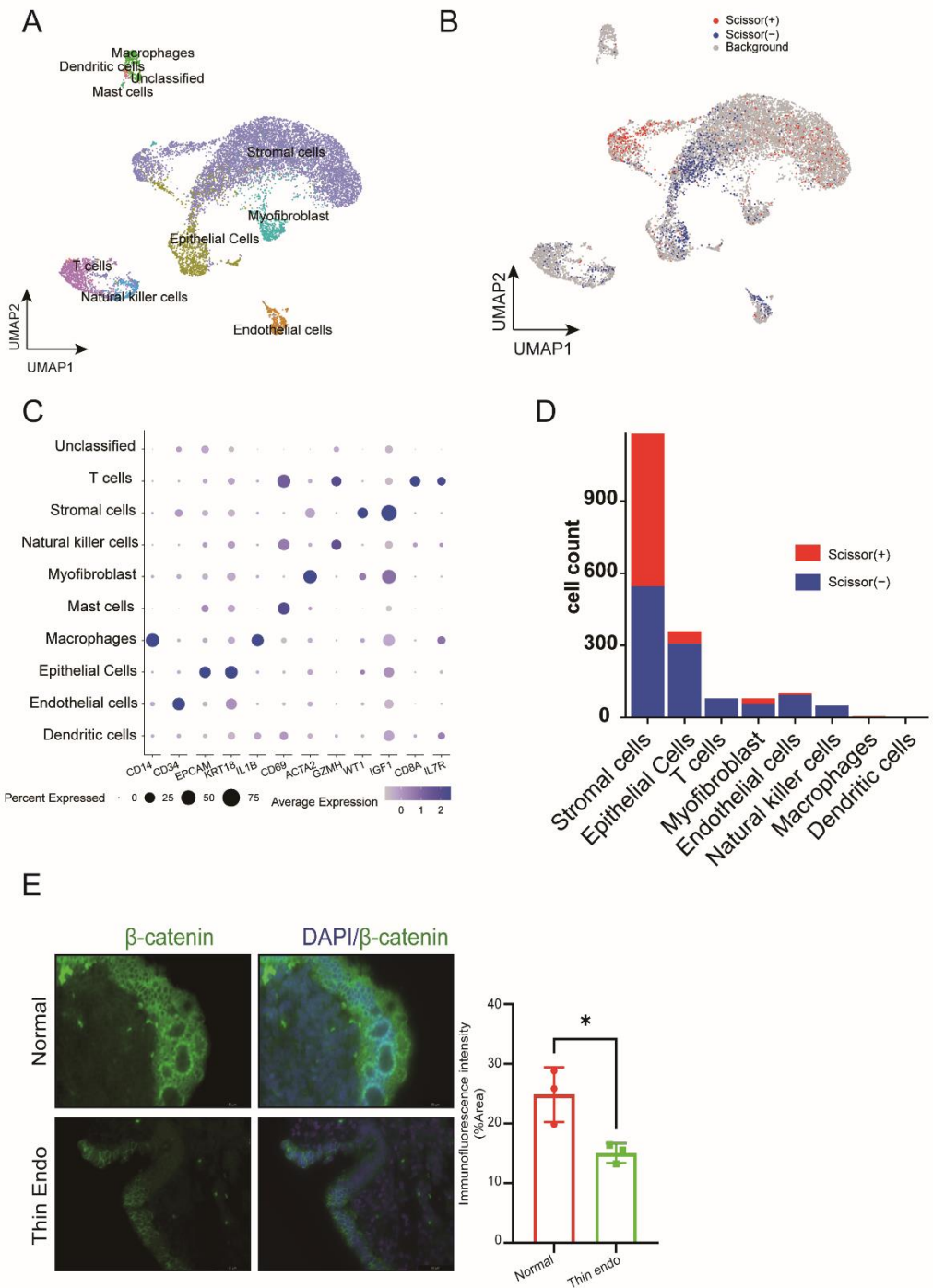


Figure S5: Distribution of the cells labeled based on the Scissor tool in thin endometrium patients.

Related to Fig. 7

(A) UMAP showing the cell types in thin and control endometria. (B) UMAP showing the distribution of the cells labeled based on the Scissor tool. The red and blue points on the right are cells associated with thin and control endometrial phenotypes, respectively. (C) Dot plot showing markers expressed in all cell populations described in SFig. 5A. (D) Bar plot showing the distribution of Scissor (+) and Scissor

(-) cells in thin endometrium patients. (E) Immunofluorescence staining to validate β -catenin expression in the endometrial luminal epithelium of normal and thin endometrium patients. Nuclei were counterstained with DAPI. The fluorescence intensity of β -catenin in the endometrial luminal epithelium was calculated by ImageJ. Scale bars: 50 μm .

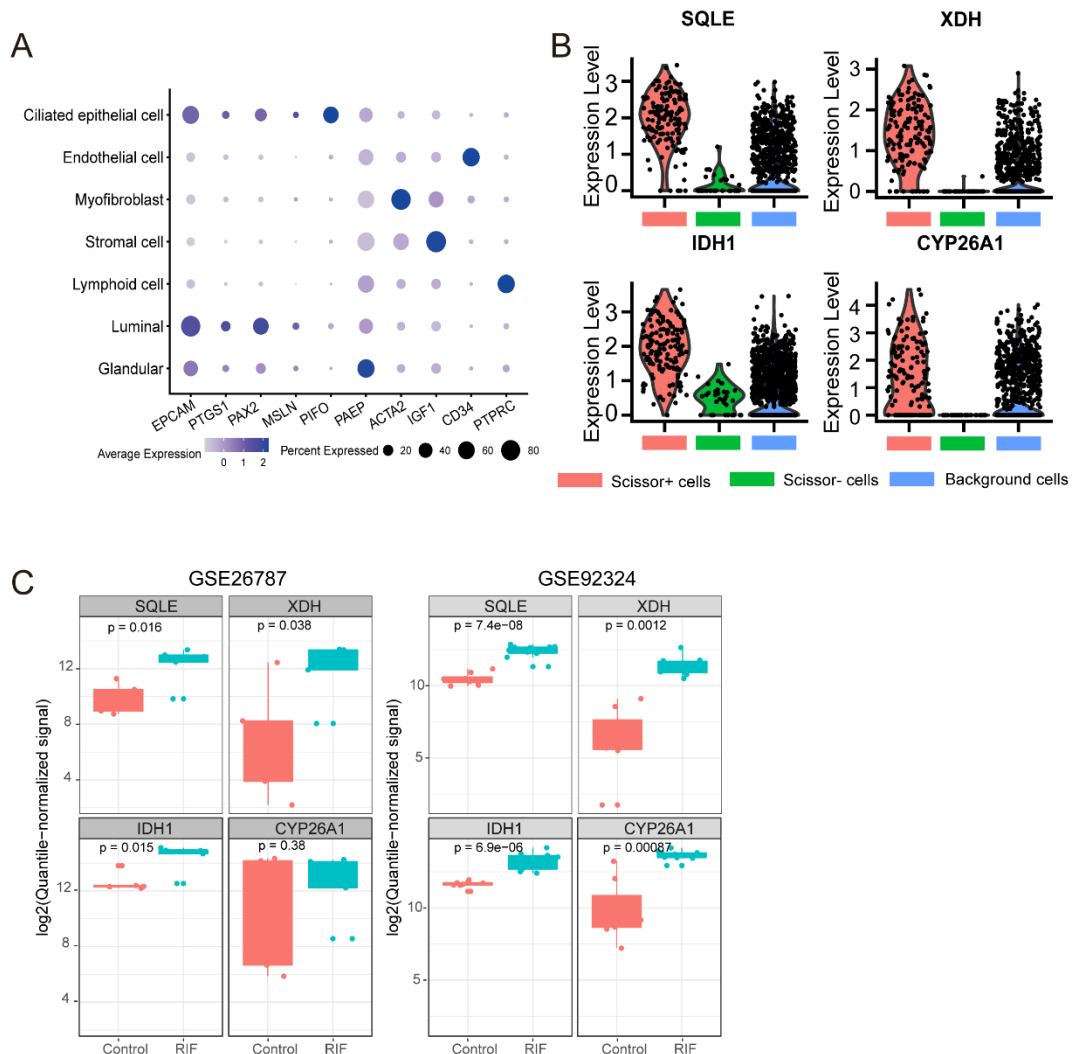


Figure S6: Distribution of the cells labeled by the Scissor tool in RIF patients. Related to Fig. 7

(A) Dot plot showing markers expressed in all cell populations described in Fig. 7E. (B) Violin plot showing the expression of genes related to sterol (CYP26A1, SQLE) and fructose (IDH1, XDH) metabolism in Scissor(+), Scissor(-) and background cells. (C) Box plot showing the expression of genes related to sterol (CYP26A1, SQLE) and fructose (IDH1, XDH) metabolism in the endometrium of normal and RIF patients in GSE92324 and GSE26787.

Effects of PDGF signals on embryo implantation

Variable	Groups		P value
	Normal Saline	Imatinib	
NO. of recipients	6	6	NS
No. of blastocysts transferred	60	60	NS
No. of implantation sites	7.33±1.63	2.67±1.97	0.0022

Note: Values are presented as mean ±SD or number (percentage). NS = nonsignificant

Effects of EphA1 on embryo implantation

Variable	Groups		P value
	siNC	siEPHA1	
NO. of recipients	5	5	NS
No. of blastocysts transferred	49	49	NS
No. of implantation sites	6.40±1.82	1.00±1.00	0.0004

Note: Values are presented as mean ±SD or number (percentage). NS = nonsignificant

Table S1. Effects of signals on embryo implantation. Related to Fig. 5 and Fig. 6

qPCR primer sequences

Gene	Forward Primer (5'-3')	Reverse Primer (5'-3')
<i>Mus musculus EphA1</i>	GTGAAGTGTATCGGGGAGCC	TCCCGTTCTTCAGAAAGGC
<i>Mus musculus Prl8a2</i>	GAGAATGGCTGCTCAGATCC	GTTCAGGTCCATGAGCTGGT
<i>Mus musculus FoxO1</i>	TCGTACGCCGACCTCATCA	CTGTCGCCCTTATCCTGAAGT
<i>Mus musculus Ltf</i>	TGATGACACCCGGAAACCTG	CGGTCGCTATGACGTACTCC
<i>Mus musculus Olfm1</i>	GTCTGGACAGGCGAACTCA	TCTTCAGTCACTGGCGCATT
<i>Mus musculus Il17rb</i>	ACTGAGAACCAACGCACTCTG	GCTACACATTAGTGAGAGCCT
<i>Mus musculus 18S rRNA</i>	ATGGCCGTTCTTAGTTGGTG	CGGACATCTAAGGGCATCAC

ISH probe amplification primer sequences

Gene	Forward Primer (5'-3')	Reverse Primer (5'-3')
<i>Mus musculus Ltf</i>	AATTAACCCTCACTAAAGGGGT ACGTCATAGCGACCGAGC	TAATACGACTCACTATAGGGACATG GTCACCCATACGCAC
<i>Mus musculus Olfm1</i>	AATTAACCCTCACTAAAGGGTTA GGTTGTGCCAGCGAG	TAATACGACTCACTATAGGGTCCC ACGATGCGTCCTTC
<i>Mus musculus Il17rb</i>	AATTAACCCTCACTAAAGGGGG ACCCAGACATCACTGCTT	TAATACGACTCACTATAGGGCGACA GACGGTGTGATGGAA
<i>Mus musculus Nudt19</i>	AATTAACCCTCACTAAAGGGTG TGTGCGCACCTAGACTG	TAATACGACTCACTATAGGGTTCC TAGGGTACACGTGCTT
<i>Mus musculus Prss29</i>	AATTAACCCTCACTAAAGGGAG TCTTCGGATCCGTGTTG	TAATACGACTCACTATAGGGTCCA GGAGCCTGTCACATT

Table S2. RT-qPCR and ISH Primers used in this article. Related to STAR

METHODS

		Patient 1			Patient 2			Patient 3		
Age (years)		31			34			32		
BMI (kg/m2)		22.57			23.38			24.44		
IVF	Date	2020/1/8	2020/4/13	2020/9/11	2019/12/19	2020/4/6	2020/7/13	2017/9/17	2019/3/13	2019/9/2
-ET	Endometrial thickness (mm)	12.3	10.9	10.2	8	8	8	14	14	12
	Embryos	1 blastocyst	1 cleavage embryo	1 cleavage embryo	1 blastocyst					
	Outcome	Nonpregna nt	Nonpregnant	Nonpregnant	Nonpregna nt					
Endocrine metabolic abnormalities		Without			Without			Without		

Table S3. Information of RIF patients. Related to STAR METHODS